A locally conservative Eulerian–Lagrangian numerical method and its application to nonlinear transport in porous media

Jim Douglas, Jr. [a], Felipe Pereira [b] and Li-Ming Yeh [c]

[a] *Department of Mathematics, Purdue University, West Lafayette, IN 47907-1395, USA*
[b] *Laboratório Nacional de Computação Científica, Petropolis, RJ, Brazil, and Instituto Politécnico da Universidade do Estado do Rio de Janeiro, Nova Friburgo, RJ, Brazil 28601-970*
[c] *Department of Applied Mathematics, National Chiao-Tung University, Hsinchu, Taiwan, R.O.C.*

Received 12 July 1999; accepted 2 November 1999

Eulerian–Lagrangian and Modified Method of Characteristics (MMOC) procedures provide computationally efficient techniques for approximating the solutions of transport-dominated diffusive systems. The original MMOC fails to preserve certain integral identities satisfied by the solution of the differential system; the recently introduced variant, called the MMOCAA, preserves the global form of the identity associated with conservation of mass in petroleum reservoir simulations, but it does not preserve a localized form of this identity. Here, we introduce an Eulerian–Lagrangian method related to these MMOC procedures that guarantees conservation of mass locally for the problem of two-phase, immiscible, incompressible flow in porous media. The computational efficiencies of the older procedures are maintained. Both the original MMOC and the MMOCAA procedures for this problem are derived from a nondivergence form of the saturation equation; the new method is based on the divergence form of the equation. A reasonably extensive set of computational experiments are presented to validate the new method and to show that it produces a more detailed picture of the local behavior in waterflooding a fractally heterogeneous medium. A brief discussion of the application of the new method to miscible flow in porous media is included.

Keywords: two-phase flow, transport-dominated diffusion processes, waterflooding, miscible flow, modified method of characteristics

AMS subject classification: 35Q60, 78-08

1. Introduction

This paper evolves from the authors' efforts [17,23,27] to develop fast, accurate, and stable versions of "Modified Method of Characteristics" numerical methods for transport-dominated diffusive systems, with the primary objective of the evolution being the incorporation of changes in these procedures to obtain the preservation of desired conservation principles. Here, we shall concentrate on the simulation of two-phase, immiscible, incompressible flows in porous media (i.e., the "waterflood

problem"); for this problem the new technique introduced herein differs significantly from earlier MMOC schemes. We shall also mention briefly in the last section the application of the new method to miscible displacement in porous media, where the new technique is quite closely related to existing MMOC procedures and to a method due to Arbogast, Chilikapati, and Wheeler [3,4,14].

The original MMOC procedure, which dates back to the late 50's though unpublished until the early 80's, provides a computationally efficient approach to many transport-dominated diffusion problems. Unfortunately, it does not preserve mass in the waterflood problem as an algebraic identity and does not necessarily preserve critical integral identities in other applications. In recent work [23,27], it was found that the error in the mass of the water phase, as computed by a standard form of the MMOC, was large enough to be comparable to that caused by the uncertainty in the physical properties of the porous medium when the geological parameters are modeled as fractals. A variant of the MMOC, called the "Modified Method of Characteristics with Adjusted Advection" (MMOCAA), was developed about three years ago and has been applied to a number of problems associated with petroleum reservoir analyses [23,24,27,31–33,36] and the transport of nuclear contaminants in porous media [43]; this method conserves mass globally (in space) at all time levels and retains all of the computational advantages of the slightly simpler MMOC. However, it does not necessarily preserve mass locally in space, and there are a number of very important physical problems for which local conservation is essential. Some of the methods labelled ELLAM [10,15] do provide the desired local conservation in an Eulerian-Lagrangian setting, but at a computational cost that is several times that of the MMOC or MMOCAA.

Here, we shall introduce a family of locally conservative Eulerian-Lagrangian methods, denoted here generically by LCELM, that again retain the computational efficiency of the MMOC and MMOCAA techniques. There is a fundamental difference between the MMOC and MMOCAA techniques and the LCELM procedure; MMOC and MMOCAA procedures consider the partial differential system (or, at least, the parabolic-type equations in the system) in nondivergence form and make use of the characteristics associated with the first-order transport part of the system in a fractional step procedure that splits the transport from the diffusive part of the system, as will be discussed in section 4 below. In contrast, the LCELM method will relate to the divergence form of the equations and then will split the transport from the diffusion. It is the use of the divergence form that allows the localization of the transport so that the desired conservation property can also be localized.

The computational results that we shall present indicate that the LCELM provides a better picture of the local behavior of the solution of the waterflood problem in reservoirs having quite inhomogeneous permeability distributions than can be obtained through MMOCAA calculations with equal spatial and temporal discretizations; this better approximation of local behavior shows the bypassing of oil in regions of low permeability somewhat more clearly than can be seen from MMOCAA simulations. Moreover, the LCELM shows a faster convergence rate of the approximate solution

than the MMOCAA, which is in turn much faster than the MMOC. Indeed, the tests that have been made with the MMOCAA frequently indicate that the same accuracy is achieved by the MMOCAA with less than 10% of the computational effort required by the MMOC in two-dimensional problems, with the implication of an even better performance ratio for three-space problems. Thus, an even greater reduction in computational effort to obtain local accuracy and conservation is available through the LCELM technique to be presented below.

A sufficient set of comparisons will be given for MMOC, MMOCAA, and LCELM techniques for the waterflood problem to validate the new LCELM procedure; recall that asymptotic convergence results have been given for both MMOC and MMOCAA applications to waterflood and other problems [16,17,24,25,28–30,36,41–43]. Analyses of the convergence of various applications of the LCELM to a collection of transport-dominated diffusion processes will be considered in the very near future. No comparisons are given here between the LCELM and ELLAM procedures; it is hoped that such comparisons can be obtained soon.

Essentially all of the applications of any of the Eulerian-Lagrangian techniques, such as the various versions of MMOC and ELLAM, concern systems of nonlinear partial differential equations of degenerate parabolic type.

2. The waterflood problem

Now, let us begin the discussion of the waterflood problem. The equations for two-phase, immiscible, incompressible flow in porous media take the form [12]

$$\Phi(x)\frac{\partial S(x,t)}{\partial t} - \operatorname{div}\big(K\Lambda\Lambda_{\mathrm{w}}(S)\nabla_x\Psi_{\mathrm{w}}(x,t)\big) = q_{\mathrm{ext,w}}(x,S), \tag{2.1a}$$

$$-\Phi(x)\frac{\partial S(x,t)}{\partial t} - \operatorname{div}\big(K\Lambda\Lambda_{\mathrm{o}}(S)\nabla_x\Psi_{\mathrm{o}}(x,t)\big) = q_{\mathrm{ext,o}}(x,S), \tag{2.1b}$$

$$P_{\mathrm{c}}(S) = \Psi_{\mathrm{c}}(x,t) + (\rho_{\mathrm{o}} - \rho_{\mathrm{w}})gz,\ \ \Psi_{\mathrm{c}}(x,t) = \Psi_{\mathrm{o}}(x,t) - \Psi_{\mathrm{w}}(x,t), \tag{2.1c}$$

for $x \in \Omega$, where Φ is the porosity, S the water saturation, and K the absolute permeability tensor of the media. The total mobility is defined as

$$\Lambda = \frac{K_{\mathrm{rw}}(S)}{\mu_{\mathrm{w}}} + \frac{K_{\mathrm{ro}}(S)}{\mu_{\mathrm{o}}},$$

where $K_{\mathrm{r}\alpha}$ is the relative permeability and μ_α the viscosity of the α-phase, $\alpha = \mathrm{w}, \mathrm{o}$. The phase mobilities are given by

$$\Lambda\Lambda_\alpha(S) = \frac{K_{\mathrm{r}\alpha}(S)}{\mu_\alpha}, \quad \alpha = \mathrm{w}, \mathrm{o};$$

Ψ_α is the α-phase potential; $q_{\mathrm{ext},\alpha}(= q_{\mathrm{ext},\alpha}(x,t,S))$ is the volumetric rate of the external source for the α-phase; $P_{\mathrm{c}} = P_{\mathrm{c}}(S) = P_{\mathrm{o}} - P_{\mathrm{w}}$ is the capillary pressure (note that

$P_{\mathrm{c}}' < 0$); ρ_α is the (constant) density of the α-phase; g is the gravitational constant; and z is the depth. Pressures are related to potentials by the relations

$$\Psi_\alpha = P_\alpha - \rho_\alpha g z, \quad \alpha = \mathrm{w}, \mathrm{o}.$$

The relative permeability functions $K_{\mathrm{r}\alpha}$ and the capillary pressure P_{c} are assumed in this paper to be independent of x; in a stratified medium these functions would be discontinuous across the interfaces between rock types, thereby imposing certain consistency conditions across these interfaces. We prefer to defer the treatment of these complications to a later presentation.

If the global pressure [2,11,12] given by

$$P := \frac{1}{2}\left(P_{\mathrm{o}} + P_{\mathrm{w}} + \int_0^{P_{\mathrm{c}}} \left[\Lambda_{\mathrm{o}}\big(P_{\mathrm{c}}^{-1}(\zeta)\big) - \Lambda_{\mathrm{w}}\big(P_{\mathrm{c}}^{-1}(\zeta)\big)\right] \mathrm{d}\zeta \right) \tag{2.2}$$

is introduced, the governing equations (2.1) can be written as a uniformly elliptic equation for global pressure and a convection-dominated parabolic equation for water saturation as follows:

$$U = -K(x)\Lambda(S)\big(\nabla P - (\Lambda_{\mathrm{w}}\rho_{\mathrm{w}} + \Lambda_{\mathrm{o}}\rho_{\mathrm{o}})g\nabla z\big), \tag{2.3a}$$

$$\operatorname{div} U = q, \tag{2.3b}$$

$$\Phi\frac{\partial S}{\partial t} + \operatorname{div}(U\Lambda_{\mathrm{w}}) + \operatorname{div}\big[(K\Lambda\Lambda_{\mathrm{w}}\Lambda_{\mathrm{o}})\big(\nabla P_{\mathrm{c}} + (\rho_{\mathrm{w}} - \rho_{\mathrm{o}})g\nabla z\big)\big] = q^+ - \Lambda_{\mathrm{w}} q^-, \tag{2.3c}$$

where $q = q_{\mathrm{ext,w}} + q_{\mathrm{ext,o}}$, $q^+ = \max(q, 0)$ and $q^- = \max(-q, 0)$. The right-hand side of (2.3c) results from assuming that only water is injected and, at a production point, the flow splits according to mobilities between water and oil.

We shall assume "no flow" boundary conditions on $\partial\Omega$:

$$U \cdot \vec{n}\,|_{\partial\Omega} = 0, \tag{2.4a}$$

$$K\Lambda\Lambda_{\mathrm{w}}\Lambda_{\mathrm{o}}\big(\nabla P_{\mathrm{c}} + (\rho_{\mathrm{w}} - \rho_{\mathrm{o}})g\nabla z\big) \cdot \vec{n}\,|_{\partial\Omega} = 0, \tag{2.4b}$$

where $\vec{n}$ is the unit outward normal vector to $\partial\Omega$. Compatibility to the incompressibility of the fluids requires that

$$\int_\Omega q\,\mathrm{d}x = 0. \tag{2.5}$$

The initial condition of the system is determined by the single relation

$$S(x, 0) = S_{\mathrm{init}}(x), \quad \text{for } x \in \Omega. \tag{2.6}$$

It will be convenient in the discussion of MMOC procedures to express the saturation equation (2.3c) in nondivergence form; a short calculation shows that

$$\begin{aligned} &\Phi\frac{\partial S}{\partial t} + \Lambda_{\mathrm{w}}'(S)U \cdot \nabla S - \operatorname{div}\left(K D(x, S)\left(\nabla S + \frac{(\rho_{\mathrm{w}} - \rho_{\mathrm{o}})g\nabla z}{P_{\mathrm{c}}'} \right) \right) \\ &\quad = (1 - \Lambda_{\mathrm{w}})q^+, \end{aligned} \tag{2.7}$$

where

$$D(x, S) = -\big(\Lambda\Lambda_{\mathrm{w}}\Lambda_{\mathrm{o}}P_{\mathrm{c}}'\big)(S). \tag{2.8}$$

It has been known for at least forty years that straightforward time discretization does not work well for convection-dominated problems, which typically develop sharp fronts in their solutions. Numerous methods have been introduced to face this problem, including the MMOC, MMOCAA, and ELLAM techniques alluded to above. Additional techniques, among many others, include higher-order Godunov schemes [6], streamline-diffusion methods [37], and the characteristics-mixed method [4]. Each of these methods has its advantages and disadvantages. The MMOC is able to capture sharp fronts and is fast, but, since it does not conserve mass, the sharp fronts are not necessarily correctly located; also, handling boundary conditions can lead to complications [26,29]. Godunov schemes need to satisfy Courant–Friedrichs–Lewy (CFL) conditions. Streamline-diffusion methods add some bias in the direction of the streamline. For ELLAM, it can be difficult to evaluate the resulting space–time equations. The characteristics-mixed method as presented in [4] is good for linear transport problems. The MMOCAA is based on MMOC and is able to capture sharp fronts while remaining fast; however, it conserves mass only globally and can miss some local behavior in the solution of the waterflood or another problem.

The LCELM technique that we shall introduce here will be fast and able to capture sharp fronts; it will automatically handle "no flow" boundary conditions and, foremost, it will conserve mass element-by-element in a natural sense. For the waterflood problem, the fundamental philosophy of the LCELM concept is based on discretization of the same operator splitting of the differential system (2.3b)–(2.3c) as is used in deriving MMOC and MMOCAA techniques for the problem. We shall retain the two-stage splitting of the MMOC and MMOCAA procedures by first splitting the approximation of the global pressure from the saturation and then splitting the transport and diffusive parts of the saturation calculation. In particular, this will allow us to retain the use of different time steps for the pressure and the saturation [18,21], along with the microstepping of the transport with respect to the diffusion [23]. In the procedure to be detailed in this paper, both the pressure and the saturation will be approximated in mixed finite element spaces; only the simplest Raviart–Thomas space [38,40,44] will be discussed here, but it will be clear that other mixed finite element spaces (e.g., [7–9,13]) could be employed. The fundamental contribution of the LCELM is in the introduction of a new time discretization for the transport microstep. This discretization is based on developing predecessor sets for each set in the finite element partition of the domain at each time microstep and a corresponding tube connecting the element and its predecessor, as does the method of Arbogast and Wheeler [4]; however, only in the case of a linear convection–diffusion equation do our tubes reduce to flow tubes, as they do in [4]. It is the difference in the definition of the tubes that allows us to treat nonlinear problems, such as the waterflood problem of this paper. The diffusive step automatically conserves mass locally as a consequence of the use of a mixed method, so that the overall time step for the saturation then

conserves mass locally. Our locally conservative discretization for transport differs significantly in concept from that arising in ELLAM procedures [15], as well as from the discretizations in the MMOC and MMOCAA techniques, which fail to be locally conservative.

Some technical aspects of the LCELM procedure of this paper which are shared with those discussed in [23] for the MMOCAA can be pointed out. Applications of quadrature reduce the equations for the pressure and the diffusive fractional step for the saturation to generalized finite volume methods, and the algebraic elimination of flux variables and Lagrange multipliers leaves both equations as cell-centered finite differences. It is simple to recover the eliminated variables (without having to store them), so that they can be used implicitly in the construction of iterative processes that can be used to solve the algebraic systems generated in both the pressure calculation and the diffusive stage of the saturation calculation.

The paper is laid out as follows. In section 3, the two-level operator splitting for the differential system is described, first to split the pressure from the saturation and then to define the two fractional steps of transport and diffusion for the saturation. Next, in section 4 the MMOC will be recast in line with this operator splitting. Then, in section 5 the LCELM procedure will be described in a differential setting. The finite element spaces to be used for spatial discretization will be introduced in section 6. Then, section 7 gives details of the discrete LCELM transport step, section 8 the diffusive saturation step, and section 9 the pressure calculation. In section 10, some technical issues related to implementing the transport microstep are given. The next, rather long section (section 11) describes a set of computational experiments. After some general remarks concerning the experiments, we first present numerical simulations intended to justify the new method through mesh refinement studies of waterflood problems for several reservoir geometries with both homogeneous and inhomogeneous permeability fields. Then, a collection of comparisons between simulations using MMOC, MMOCAA, and LCELM methods are given to indicate the superiority of the computed results for the LCELM approach. Finally, section 12 contains a brief description of the application of the LCELM to miscible flow in porous media.

3. The basic operator splitting

Let [21,23]

$$\Delta t_{\mathrm{p}} = i_1 \Delta t_{\mathrm{s}} = i_1 i_2 \Delta t_{\mathrm{st}} > 0, \tag{3.1}$$

where i_1 and i_2 are positive integers; Δt_{p} will be the time step for the pressure calculation, Δt_{s} the time step for the diffusive stage saturation calculation, and Δt_{st} the microstep for the transport stage saturation calculation. Let discrete times be given by

$$t^m = m\Delta t_{\mathrm{p}}, \qquad t_n = n\Delta t_{\mathrm{s}}, \qquad t_{n,\kappa} = t_n + \kappa \Delta t_{\mathrm{st}}; \tag{3.2}$$

the normal range for κ is $0 \leqslant \kappa \leqslant i_2$, though on occasion it will be convenient to use κ outside that range. Given a function f, we shall denote its value at time t^m by f^m,

at time t_n by f_n, and at $t_{n,\kappa}$ by $f_{n,\kappa}$; single-valuedness in time is assumed. In practice, variable time steps, at least for Δt_{p} and Δt_{s}, are almost always useful; however, we shall leave this trivial modification in the procedures described below to the reader.

The primary operator splitting is to separate pressure and saturation. Note that the initial condition specifying $S^0 = S_{\mathrm{init}}$ allows the evaluation of P^0 and U^0. Then, let $E_1 U$ denote the extrapolation of U given by

$$(E_1U)(t) = \begin{cases} U^0, & 0 < t \leqslant t^1, \\ \dfrac{t - t^{m-1}}{\Delta t_{\mathrm{p}}} U^m - \dfrac{t - t^m}{\Delta t_{\mathrm{p}}} U^{m-1}, & t^m < t \leqslant t^{m+1}. \end{cases} \tag{3.3}$$

The general algorithm for the primary operator splitting is as follows (the "no-flow" boundary conditions are assumed to be imposed and will not be repeated except where necessary for clarity):

1. Given S^m, $m \geqslant 0$, determine (P^m, U^m) by solving the pressure equation (in mixed form)

$$U^m = -K\Lambda^m\big(\nabla P^m - \big(\Lambda_{\mathrm{w}}^m \rho_{\mathrm{w}} + \Lambda_{\mathrm{o}}^m \rho_{\mathrm{o}}\big) g \nabla z\big), \tag{3.4a}$$

$$\operatorname{div} U^m = q^m. \tag{3.4b}$$

2. For $t^m < t \leqslant t^{m+1}$, solve the saturation equation (now expressed in nondivergence, mixed form)

$$V = -K D(x,S)\left(\nabla S + \frac{(\rho_{\mathrm{w}} - \rho_{\mathrm{o}}) g \nabla z}{P_{\mathrm{c}}'}\right), \tag{3.5a}$$

$$\Phi \frac{\partial S}{\partial t} + \Lambda_{\mathrm{w}}'(S)(E_1U) \cdot \nabla S + \operatorname{div} V = (1 - \Lambda_{\mathrm{w}})\, q^+, \tag{3.5b}$$

$$S\big(x, t^m\big) = S^m(x), \tag{3.5c}$$

where, in (3.5c), $S^m(x)$ denotes the final values from the $[t^{m-1}, t^m]$-calculation or, for $m = 0$, the initial saturation.

The secondary operator splitting is defined by a fractional step procedure for carrying out the solution of (3.5a). The algorithm for this is as follows:

(1) Let $t_{n_1} = t^m$ and assume P, U, and S to be known for $t \leqslant t_{n_1}$.

(2) For $n = n_1, \ldots, n_2 = n_1 + i_1 - 1$,

(a) For $\kappa = 0, \ldots, i_2 - 1$, compute the transport over $[t_{n,k}, t_{n,\kappa+1}]$ by solving the system

$$\Phi \frac{\partial \zeta_{n,\kappa}}{\partial t} + \Lambda_{\mathrm{w}}'(\zeta_{n,\kappa})(E_1U) \cdot \nabla \zeta_{n,\kappa} = (1 - \Lambda_{\mathrm{w}})\, q^+, \quad x \in \Omega, \tag{3.6a}$$

$$(E_1U) \cdot \vec{n} = 0, \qquad x \in \partial\Omega, \tag{3.6b}$$

$$\zeta_{n,\kappa}(x, t_{n,\kappa}) = \begin{cases} S_n(x), & \kappa = 0, \\ \zeta_{n,\kappa-1}(x, t_{n,\kappa}), & \kappa = 1, \ldots, i_2 - 1. \end{cases} \tag{3.6c}$$

(b) Set $\overline{S}_n(x) = \zeta_{n,i_2-1}(x, t_{n,i_2}) = \zeta_{n,i_2-1}(x, t_{n+1})$.

(c) Compute the diffusive effects over $[t_n, t_{n+1}]$ by solving

$$V = -KD(x,S)\left(\nabla S + \frac{(\rho_{\mathrm{w}} - \rho_{\mathrm{o}})g\nabla z}{P_{\mathrm{c}}'}\right), \quad x \in \Omega, \tag{3.7a}$$

$$\Phi\frac{\partial S}{\partial t} + \operatorname{div} V = 0, \qquad x \in \Omega, \tag{3.7b}$$

$$V \cdot \vec{n} = 0, \qquad x \in \partial\Omega, \tag{3.7c}$$

$$S(x, t_n) = \overline{S}_n(x), \qquad x \in \Omega. \tag{3.7d}$$

(3) Set $S^{m+1}(x) = S_{n_2}(x, t_{n_2+1}) = S_{n_2}(x, t^m)$.

The difference between the MMOC (and MMOCAA) and the LCELM procedures for the waterflood problem, as well as in their applications to other problems, lies in the temporal discretization of the transport step (3.6) above; there are no essential differences in the treatments of the pressure or the diffusion.

4. A reinterpretation of the MMOC procedure

The MMOC procedure for the waterflood problem is based on introducing a characteristic derivative for the transport part of the saturation equation written in nondivergence form. Let

$$\Theta(x, S, U) = \sqrt{\Phi(x)^2 + \left|\Lambda_{\mathrm{w}}'(S)U\right|^2}, \tag{4.1a}$$

$$\Theta\frac{\partial}{\partial\tau} = \Phi\frac{\partial}{\partial t} + \Lambda_{\mathrm{w}}'(S)U \cdot \nabla. \tag{4.1b}$$

Note that the characteristic direction τ depends on x, the saturation, and the fluid velocity. Thus, (3.5b) can be written as

$$\Theta\frac{\partial S}{\partial\tau} + \operatorname{div} V = (1 - \Lambda_{\mathrm{w}})\, q^+, \tag{4.2}$$

and the transport microstep in the secondary operator splitting consists of solving the equation

$$\Theta\frac{\partial\zeta_{n,\kappa}}{\partial\tau} = \big(1 - \Lambda_{\mathrm{w}}(\zeta_{n,\kappa})\big)q^+, \quad x \in \Omega,\ t_{n,\kappa} < t \leqslant t_{n,\kappa+1}, \tag{4.3}$$

with initial values again given by (3.6c); see [23] for a careful treatment of some technical details. In [23] there is a different splitting of the right-hand side of (3.5b) between the transport and diffusive steps than given above, and the handling of the no-flow boundary condition is discussed. The fundamental concept in the MMOC is the discretization of the characteristic derivative by backwards differencing along the

tangent to the characteristic through the point $(x, t_{n,\kappa+1})$ back to the time level $t_{n,\kappa}$ for whatever x-points arise in the quadratures used in the finite element scheme. While the characteristics cannot leave Ω for the differential problem, thanks to the no-flow boundary condition, the tangents can cross $\partial\Omega$ and a modification must be introduced for those characteristics; see [26,29] for the remedy, which also applies when there is a source at the boundary. If we ignore for the moment sources and sinks and the boundary, the transported values over a microstep would be defined by

$$\overline{x}_{n,\kappa}(x) = x - \frac{\Lambda_{\mathrm{w}}'(\zeta_{n,\kappa})(E_1 U)(x, t_{n,\kappa+1})\Delta t_{\mathrm{st}}}{\Phi}, \tag{4.4a}$$

$$\zeta_{n,\kappa+1}(x) = \zeta_{n,\kappa}\big(\overline{x}_{n,\kappa}(x)\big). \tag{4.4b}$$

The only reasonable criterion [25] for conservation of mass globally is that the map (4.4a) have Jacobian identically one; this condition inevitably fails in more than a single space variable and a large number of numerical experiments over a couple of decades have confirmed the lack of conservation. The MMOCAA [23] is a somewhat ad hoc, though effective, perturbation to the MMOC to obtain global conservation.

5. The differential LCELM procedure

The LCELM is fundamentally tied to a local conservation relation that seems not to have been exploited before, though a related global version of it was important in the definition of the MMOCAA procedure. Recall that the saturation equation can be written in divergence form as

$$\nabla_{t,x} \cdot \begin{pmatrix} \Phi S \\ \Lambda_{\mathrm{w}} U \end{pmatrix} + \operatorname{div} V = q^+ - \Lambda_{\mathrm{w}} q^-. \tag{5.1}$$

Then, the fractional stepping procedure for it corresponds to the transport equation

$$\nabla_{t,x} \cdot \begin{pmatrix} \Phi S \\ \Lambda_{\mathrm{w}} U \end{pmatrix} = q^+ - \Lambda_{\mathrm{w}} q^-, \tag{5.2}$$

followed by the diffusive part given by

$$\Phi \frac{\partial S}{\partial t} + \operatorname{div} V = 0. \tag{5.3}$$

Consider the space–time slice $\mathcal{Q} = \Omega \times [t_{n,\kappa}, t_{n,\kappa+1}]$. Let $\mathcal{K}$ be a reasonably shaped, simply-connected subset of Ω, and define a subset $\mathcal{D} = \mathcal{D}_{n,\kappa}(\mathcal{K})$ of $\mathcal{Q}$ as follows. For each $x \in \partial\mathcal{K}$, construct the solution $y(x;t)$ of the final value problem

$$\frac{\mathrm{d}y}{\mathrm{d}t} = \frac{\Lambda_{\mathrm{w}} U}{\Phi S}, \quad t_{n,\kappa+1} > t \geqslant t_{n,\kappa}, \tag{5.4a}$$

$$y(x; t_{n,\kappa+1}) = x, \tag{5.4b}$$

and set

$$\overline{x}_{n,\kappa}(x) = y(x; t_{n,\kappa}). \tag{5.5}$$

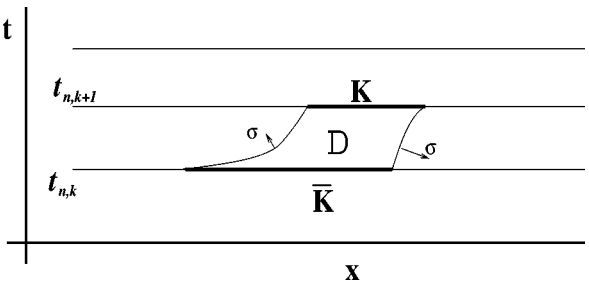

Figure 1. The space–time domain $\mathcal{D}$.

Then, let $\overline{\mathcal{K}} = \overline{\mathcal{K}}_{n,\kappa}$ be the set in $\Omega \cap \{t = t_{n,\kappa}\}$ interior to $\{\overline{x}_{n,\kappa}(x)\colon\ x \in \partial\mathcal{K}\}$, and let $\mathcal{D}$ be the tube determined by $\mathcal{K}$, $\overline{\mathcal{K}}$, and the integral curves (5.4a); see figure 1 for an example $\mathcal{D}$ in a single space variable setting. (For Δt_{st} sufficiently small, the map $x \to \overline{x}_{n,\kappa}$ is one-to-one, so that this construction can be carried out.) Now, denote the outward normal to $\partial\mathcal{D}$ by $\sigma(x,t)$ and note that it is orthogonal to the vector $(\Phi S, \Lambda_{\mathrm{w}} U)^{\mathrm{T}}$ on the lateral surface of $\mathcal{D}$. Then, integrate (5.2) over $\mathcal{D}$:

$$\begin{aligned}\int_{\mathcal{D}} \nabla_{t,x} \cdot \begin{pmatrix} \Phi S \\ \Lambda_{\mathrm{w}} U \end{pmatrix} \mathrm{d}x\,\mathrm{d}t &= \int_{\partial\mathcal{D}} \begin{pmatrix} \Phi S \\ \Lambda_{\mathrm{w}} U \end{pmatrix} \cdot \sigma \,\mathrm{d}A \\ &= \int_{\mathcal{K}} \Phi S(t_{n,\kappa+1}, x)\,\mathrm{d}x - \int_{\overline{\mathcal{K}}} \Phi S(t_{n,\kappa}, x)\,\mathrm{d}x \\ &= \int_{\mathcal{D}} \left(q^{+} - \Lambda_{\mathrm{w}} q^{-}\right) \mathrm{d}x\,\mathrm{d}t. \end{aligned} \tag{5.6}$$

Thus, mass is conserved locally in the transport step, as defined in (5.2) or (3.6a) above, if

$$\int_{\mathcal{K}} \Phi S(x, t_{n,\kappa+1})\,\mathrm{d}x = \int_{\overline{\mathcal{K}}} \Phi S(x, t_{n,\kappa})\,\mathrm{d}x + \int_{\mathcal{D}} \left(q^{+} - \Lambda_{\mathrm{w}} q^{-}\right) \mathrm{d}x\,\mathrm{d}t. \tag{5.7}$$

The no-flow boundary condition is handled in a natural way in (5.6), since the integral curves (5.4a) do not exit Ω in this case. In fact, if $x \in \partial\Omega$, then the integral curve remains in $\partial\Omega$ and $\mathcal{D}$ has a portion of its lateral surface contained in $\partial\Omega \times [t_{n,\kappa}, t_{n,\kappa+1}]$. Hence, no special cases arise for subsets $\mathcal{K}$ close to the boundary for these boundary conditions.

Another property associated with the integral curves (5.4a) should be pointed out. Since

$$\frac{\Lambda_{\mathrm{w}}(S)}{S} = 0 \quad \text{for } 0 < S \leqslant S_{\mathrm{w,res}}, \tag{5.8}$$

where $S_{\mathrm{w,res}}$ is the (positive) residual water saturation, the integral curves do not degenerate as $S \to 0$.

The characteristic curves employed in the MMOC, MMOCAA, ELLAM, and characteristics-mixed methods are given by solving the final value problems

$$\frac{\mathrm{d}y}{\mathrm{d}t} = \frac{\Lambda_{\mathrm{w}}' U}{\Phi}, \quad t_{n,\kappa+1} > t \geqslant t_{n,\kappa}, \tag{5.9a}$$

$$y(x; t_{n,\kappa+1}) = x; \tag{5.9b}$$

thus, the integral curves used in the LCELM procedure differ from the characteristic curves appearing in these other techniques unless Λ_{w} is linear, as it is in the case of miscible displacement rather than immiscible. The tube $\mathcal{D}$ is associated with the transport of mass, while the tube that would be generated by use of the characteristics, as in [4], is associated with the transport of saturation; that these are not equivalent was pointed out in [23].

The integral curves used in the discrete LCELM procedure will be associated with points on the boundary (usually vertices) of the finite elements; typically, the characteristic curves in the other techniques are associated with quadrature points in the interiors of the finite elements. The characteristics arising in the ELLAM procedure for the waterflood problem (see [15]) are somewhat different from what would be employed in a linear problem, since the transport is split into two pieces. In fact, in [15] only global mass conservation is claimed.

5.1. *A characteristics-based procedure in differential form*

For the purpose of comparison with the LCELM procedure just described, we shall now indicate a locally conservative scheme, in differential form, which is based upon the use of characteristics for constructing the space–time tubes.

The transport equation in nondivergence form can be written as

$$\nabla_{t,x} \cdot \begin{pmatrix} \Phi S \\ S\Lambda_{\mathrm{w}}' U \end{pmatrix} - S\nabla \cdot \left(\Lambda_{\mathrm{w}}' U\right) = (1 - \Lambda_{\mathrm{w}}) q^{+}. \tag{5.10}$$

Consider, as in the LCELM procedure, the space–time slice $\mathcal{Q} = \Omega \times [t_{n,\kappa}, t_{n,\kappa+1}]$. Let $\mathcal{K}$ be a simply connected subset of Ω, and define a subset $\mathcal{D} = \mathcal{D}_{n,\kappa}(\mathcal{K})$ of $\mathcal{Q}$ as follows. For each $x \in \partial\mathcal{K}$, construct the solution $y(x;t)$ of the final value problem

$$\frac{\mathrm{d}y}{\mathrm{d}t} = \frac{\Lambda_{\mathrm{w}}' U}{\Phi}, \quad t_{n,\kappa+1} > t \geqslant t_{n,\kappa}, \tag{5.11a}$$

$$y(x; t_{n,\kappa+1}) = x, \tag{5.11b}$$

and set

$$\overline{x}_{n,\kappa}(x) = y(x; t_{n,\kappa}). \tag{5.12}$$

Then, let $\overline{\mathcal{K}} = \overline{\mathcal{K}}_{n,\kappa}$ be the set in $\{t = t_{n,\kappa}\}$ interior to $\{\overline{x}_{n,\kappa}(x)\colon\ x \in \partial\mathcal{K}\}$, and let $\mathcal{D}$ be the "characteristic" tube determined by $\mathcal{K}$, $\overline{\mathcal{K}}$, and the integral curves (5.11a).

Now, denote the outward normal to $\partial\mathcal{D}$ by $\sigma(x,t)$ and note that it is orthogonal to the vector $(\Phi, \Lambda_{\mathrm{w}}' U)^{\mathrm{T}}$ on the lateral surface of $\mathcal{D}$. Then, integrate (5.10) over $\mathcal{D}$ to obtain

$$\int_{\mathcal{K}} \Phi S(x, t_{n,\kappa+1})\,\mathrm{d}x = \int_{\overline{\mathcal{K}}} \Phi S(x, t_{n,\kappa})\,\mathrm{d}x + \int_{\mathcal{D}} (1-\Lambda_{\mathrm{w}}) q^{+}\,\mathrm{d}x\,\mathrm{d}t + \int_{\mathcal{D}} S\nabla\cdot\left(\Lambda_{\mathrm{w}}' U\right)\mathrm{d}x\,\mathrm{d}t. \quad (5.13)$$

Note that in the development of a numerical method based on (5.13) the last term in this equation would have to be accurately approximated, and this seems to be computationally difficult. Indeed, whether the integrand of that term is considered as $S\nabla\cdot(\Lambda_{\mathrm{w}}' U)$ or as $S\Lambda_{\mathrm{w}}' q + S\Lambda_{\mathrm{w}}'' U\cdot\nabla S$, it generates a distribution on the interfaces between the elements, and the evaluation of the term to the same level of accuracy as can be obtained in the LCELM poses a severe problem. In fact, the main advantage of the LCELM procedure over one based on (5.13) is the fact that such a term does not appear in the scheme.

6. Spatial discretization by mixed finite elements

Let us return to the differential system (2.3a) and restate it completely in mixed form by introducing a saturation flux variable in addition to the volumetric flow rate variable U. Then, the equations take the form

$$U = -K(x)\Lambda(S)\big(\nabla P - (\Lambda_{\mathrm{w}}\rho_{\mathrm{w}} + \Lambda_{\mathrm{o}}\rho_{\mathrm{o}})g\nabla z\big), \quad (6.1a)$$

$$\operatorname{div} U = q, \quad (6.1b)$$

$$V = -KD(x,S)\left(\nabla S + \frac{(\rho_{\mathrm{w}}-\rho_{\mathrm{o}})g\nabla z}{P_{\mathrm{c}}'}\right), \quad (6.1c)$$

$$\Phi\frac{\partial S}{\partial t} + \operatorname{div}(\Lambda_{\mathrm{w}} U) + \operatorname{div} V = q^{+} - \Lambda_{\mathrm{w}} q^{-}. \quad (6.1d)$$

It should be noted that gravity terms enter into both flux variables. The no-flow boundary conditions are expressed by

$$U\cdot\vec{n} = V\cdot\vec{n} = 0, \quad x\in\partial\Omega. \quad (6.2)$$

We wish to approximate each pair, (U,P) and (V,S), by mixed finite elements. It is completely feasible and can be computationally advantageous [19,20] to define the finite element methods for the pressure equation and the saturation equation over different partitions of the domain, but in order to simplify our presentation we shall restrict our considerations to the use of the same partition for the two sets of variables. Moreover, we shall take the domain Ω to be a rectangle in the plane partitioned into uniform squares and employ the simplest Raviart–Thomas rectangular elements [40] over this partition. The ideas that will be described in detail for these choices carry over to three-dimensional domains and to simplicial mixed elements in either dimension without conceptual difficulties, provided that P and S are approximated by

constants on each element. Elements that are higher order in the scalar variable would require some nontrivial modifications in the method.

Let

$$\Omega = [0, L_x] \times [0, L_y],$$

and set $H = (H_x, H_y)$, where $H_x = L_x/N_x$ and $H_y = L_y/N_y$. Then, let $X_i = iH_x$ and $Y_j = jH_y$, and define the elements of the partition $\mathcal{T} = \mathcal{T}(H) = \{M_{ij}\colon\ i = 1, \ldots, N_x, j = 1, \ldots, N_y\}$ by $M_{ij} = [X_{i-1}, X_i] \times [Y_{j-1}, Y_j]$; $\mathcal{T}$ will serve for both the pressure and the saturation equations. Let

$$\mathcal{V} = \mathcal{V}(H) = \left\{\vec{v} \in H(\text{div}, \Omega)\colon\ \vec{v}\,|_{M_{ij}} \in \mathcal{P}_{1,0} \times \mathcal{P}_{0,1} \text{ and } \vec{v} \cdot \vec{n} = 0 \text{ on } \partial\Omega\right\},$$

$$W = W(H) = \{w\colon\ w|_{M_{ij}} \in P_0\} \subset L^2(\Omega),$$

where P_k denotes the set of polynomials of total degree k and $\mathcal{P}_{k,\ell}$ denotes the tensor product of polynomials of degree k in x by those of degree ℓ in y. Then, set

$$\mathcal{M} = \mathcal{M}(H) = \mathcal{V} \times W;$$

i.e., the lowest index Raviart–Thomas mixed finite element space over the partition $\mathcal{T}$.

We shall seek an approximate solution to the system (6.1a) such that (we shall employ the notation $(\mathbf{U}, \mathbf{P})$ and $(\mathbf{V}, \mathbf{S})$ and $\mathbf{z}$ in place of ζ in the solution of the fully discrete system)

1. $(\mathbf{U}^m, \mathbf{P}^m) \in \mathcal{M},\ m = 0, 1, \ldots.$
2. $(\mathbf{V}_n, \mathbf{S}_n) \in \mathcal{M},\ n = 0, 1, \ldots.$
3. $\mathbf{z}_{n,\kappa} \in W,\ n = 0, 1, \ldots,\ \kappa = 0, \ldots, i_2 - 1.$

The implementation of the spatially discretized LCELM procedure will be given next, with the critical, new transport microstep being described first.

7. The LCELM transport microstep

The fundamental questions are the choices of the discrete analogues $\mathbf{K}$ of the sets $\mathcal{K}$ discussed in section 5 and the procedure for defining the analogue $\overline{\mathbf{K}}$ of $\overline{\mathcal{K}}$. Consider first the choice of $\{\mathbf{K}\}$; in each possibility discussed below, $\overline{\mathbf{K}}(\mathbf{K})$ should remain a subset of Ω, given the no-flow boundary condition. The authors considered the following choices:

1. For each $M_{ij} \in \mathcal{T}$, let $\mathbf{K}_{ij} = M_{ij}$.
2. For each $M_{ij} \in \mathcal{T}$, associate a cell-centered rectangle $\mathbf{K}_{ij}$ overlapping M_{ij} and its three neighbors to the left and below.
3. For each $M_{ij} \in \mathcal{T}$, divide M_{ij} into four equal rectangles $\mathbf{K}_{i,j,k},\ k = 1, \ldots, 4$.
4. For each $M_{ij} \in \mathcal{T}$, divide M_{ij} into four triangles $\mathbf{K}_{i,j,k},\ k = 1, \ldots, 4$, by diagonals.

Calculations were made using the first two choices. The second choice induces some artificial diffusion and was discarded. The third and fourth choices would appear to lead to more accurate transport, but the fourth would produce exactly the same $\mathbf{z}_{n,\kappa}$-values as the first choice, since the union of the four sets $\overline{\mathbf{K}}_{i,j,k}$ would coincide with the single predecessor set of the first choice. The union of the four $\overline{\mathbf{K}}_{i,j,k}$ sets for the third choice would not, in general, coincide with the single $\overline{\mathbf{K}}_{ij}$ of the first choice if the predecessor sets are defined by integral curves (5.4a) associated with the vertices of $\mathbf{K}_{i,j,k}$ and $\mathbf{K}_{ij}$; hence, the third choice could give improved approximate transport. The experimental results reported in section 11 are all based on the use of the first choice, and only this choice will be detailed below.

We shall require an interpretation for $E_1\mathbf{U}$, since the Raviart–Thomas flux $\mathbf{U}^m$ is discontinuous at vertices of the elements. Two choices appear feasible. The simplest would be to average the two x-component values and the two y-component values at time t^m; the second is to interpolate cell-center fluxes bilinearly and then evaluate this continuous vector function at vertices. Then, apply the extrapolation operator E_1. The second procedure is preferable, as it treats all four elements surrounding a vertex equally in the evaluation of both components of $\mathbf{U}$ and, in the case of smooth coefficients in the differential system, gives a continuous, second-order correct approximation of the velocity field (see [16,17,20]); thus, it would be useful for a more accurate determination of $\partial\overline{\mathbf{K}}_{ij}$ than the procedure to be outlined below. It is the method used in all but one of the calculations in section 11; the first method is employed in that single case for a comparison. (Near $\partial\Omega$, the no-flow condition can be interpreted through reflection.) Denote the bilinearly interpolated $\mathbf{U}^m$ by $\widetilde{\mathbf{U}}^m$. Similarly, denote the corresponding cell-centered bilinear interpolations of $\mathbf{z}_{n,\kappa}$ and $\mathbf{S}_n$ by $\widetilde{\mathbf{z}}_{n,\kappa}$ and $\widetilde{\mathbf{S}}_n$, respectively.

So, let $\mathbf{K}_{ij} = M_{ij}$. We shall define $\overline{\mathbf{K}}_{ij}$ as the quadrilateral obtained by approximating the integral curves (5.4a) at the vertices $x_{i,j,k}$, $k = 1,\ldots,4$, of $\mathbf{K}_{ij}$. Since the microstep Δt_{st} is usually small (i.e., $i_2 = 10$ or so) with respect to Δt_{s}, it should suffice to follow the tangent to the integral curve through $(x_{i,j,k}, t_{n,\kappa+1})$ back to the time level $t_{n,\kappa}$. In order to do so, it is necessary to have a good approximation of the saturation at $(x_{i,j,k}, t_{n,\kappa+1})$; now, here we can apply a standard MMOC transport related to the function $\mathbf{z}_{n,\kappa}$ as follows. Let

$$\widetilde{\mathbf{x}}_{i,j,k,n,\kappa} = x_{i,j,k} - \frac{\Lambda'_{\mathrm{w}}(\mathbf{z}_{n,\kappa}(x_{i,j,k}))(E_1\widetilde{\mathbf{U}})(x_{i,j,k}, t_{n,\kappa+1})\Delta t_{\mathrm{st}}}{\Phi}, \tag{7.1a}$$

$$\overline{\mathbf{z}}_{i,j,k,n,\kappa} = \widetilde{\mathbf{z}}_{n,\kappa}(\widetilde{\mathbf{x}}_{i,j,k,n,\kappa}), \tag{7.1b}$$

$$\overline{\mathbf{x}}_{i,j,k,n,\kappa} = x_{i,j,k} - \frac{\Lambda_{\mathrm{w}}(\overline{\mathbf{z}}_{i,j,k,n,\kappa})(E_1\widetilde{\mathbf{U}})(x_{i,j,k}, t_{n,\kappa+1})\Delta t_{\mathrm{st}}}{\Phi\overline{\mathbf{z}}_{i,j,k,n,\kappa}}. \tag{7.1c}$$

For sufficiently small Δt_{st}, the four points $\overline{\mathbf{x}}_{i,j,k,n,\kappa}$, $k = 1,\ldots,4$, form the vertices of a quadrilateral, $\overline{\mathbf{K}}_{ij} = \overline{\mathbf{K}}_{i,j,n,\kappa}$, which intersects at most the nine elements $M_{\alpha\beta}$, $i-1 \leqslant \alpha \leqslant i+1$, $j-1 \leqslant \beta \leqslant j+1$.

Next, we must discretize the local conservation relation (5.7). In the waterflood problem, it is quite reasonable to assume that the porosity Φ is constant over each element $M_{\alpha\beta}$, given the uncertainties in the reservoir data; in fact, since the saturation is being approximated only to first order in H, averaging Φ over each element is consistent with the discretization. Having both the saturation variable and the porosity as piecewise constants allows us to evaluate the integrals over $\mathbf{K}_{ij}$ and $\overline{\mathbf{K}}_{ij}$ exactly (see section 10 below). This leaves the integral of $\Lambda_{\mathrm{w}}q$ over the tube $\mathbf{D}_{ij}$ connecting $\mathbf{K}_{ij}$ and $\overline{\mathbf{K}}_{ij}$. Now, it is clear that

$$\bigl|\overline{\mathbf{K}}_{ij}\bigr| = \bigl(1 + \mathcal{O}(\Delta t_{\mathrm{st}})\bigr)|\mathbf{K}_{ij}|$$

and that the shape quasiregularity constant associated with the map $\mathbf{K}_{ij} \to \overline{\mathbf{K}}_{ij}$ is also $1 + \mathcal{O}(\Delta t_{\mathrm{st}})$; consequently, applying the trapezoidal rule in time to this space–time integral is adequate to maintain accuracy to order $\mathcal{O}((\Delta t_{\mathrm{st}})^3)$ over a microstep, which indicates that the mass balance error generated by this quadrature is essentially of the same size as that generated by using the quadrilateral $\overline{\mathbf{K}}_{ij}$ in place of the predecessor that would be obtained by tracing back the entire boundary of $\mathbf{K}_{ij}$. Thus, we are led to the conservation relation

$$\int_{\mathbf{K}_{ij}} \Phi \mathbf{z}_{n,\kappa+1}\,\mathrm{d}x = \int_{\overline{\mathbf{K}}_{ij}} \Phi \mathbf{z}_{n,\kappa}\,\mathrm{d}x + \frac{\Delta t_{\mathrm{st}}}{2}\biggl(\int_{\mathbf{K}_{ij}} \bigl(q^+ - \Lambda_{\mathrm{w}}(\mathbf{z}_{n,\kappa+1})q^-\bigr)\,\mathrm{d}x + \int_{\overline{\mathbf{K}}_{ij}} \bigl(q^+ - \Lambda_{\mathrm{w}}(\mathbf{z}_{n,\kappa})q^-\bigr)\,\mathrm{d}x\biggr).$$

If $\mathbf{z}_{i,j,n,\kappa}$ denotes the value of $\mathbf{z}_{n,\kappa}$ on M_{ij}, then the equation above is equivalent to the simple nonlinear equation

$$\begin{aligned}\Phi|\mathbf{K}_{ij}|\mathbf{z}_{i,j,n,\kappa+1} &+ \biggl(\frac{\Delta t_{\mathrm{st}}}{2}\int_{\mathbf{K}_{ij}} q^-\,\mathrm{d}x\biggr)\Lambda_{\mathrm{w}}(\mathbf{z}_{i,j,n,\kappa+1}) \\ &= \int_{\overline{\mathbf{K}}_{ij}} \Phi \mathbf{z}_{n,\kappa}\,\mathrm{d}x + \frac{\Delta t_{\mathrm{st}}}{2}\biggl(\int_{\mathbf{K}_{ij}} + \int_{\overline{\mathbf{K}}_{ij}}\biggr) q^+\,\mathrm{d}x - \frac{\Delta t_{\mathrm{st}}}{2}\int_{\overline{\mathbf{K}}_{ij}} \Lambda_{\mathrm{w}}(\mathbf{z}_{n,\kappa})q^-\,\mathrm{d}x. \quad (7.2)\end{aligned}$$

Solving (7.2) on each element $M_{ij} = \mathbf{K}_{ij}$ completes the transport microstep in the saturation calculation. Note that (7.2) is a linear equation except on elements containing production. We would like to emphasize that the right-hand side of (7.2) can and should be evaluated exactly.

Some observations are in order. First, this is an explicit calculation, element-by-element. Second, in the waterflood problem q will vanish on almost all elements, so that the nonlinearity goes away on the vast majority of the elements. And, if the sources and sinks are considered to be concentrated at points (as they certainly would be in anything but a laboratory experiment) or if they are considered to be uniformly distributed over a single element, then the evaluation of the integrals of the source and sink terms in (7.2) is either trivial or relatively simple; see section 10. Third, the transport microstep remains very quick, so that the computational efficiency of the MMOC and MMOCAA procedures has been retained.

For elements containing an injection point, (7.2) can generate a constraint on Δt_{st}. This problem can be avoided through locally refining the microstep in the neighborhood of the injection point without inducing a time step limitation over the whole domain. However, in the experimental calculations reported in section 11 no time step reduction was required by an overshoot at injection points, presumably because the time steps were sufficiently small as to avoid the need for a reduction.

8. The LCELM diffusive fractional step for the saturation

Consider the diffusive fractional time step for $\mathbf{S}_{n+1}$; as a result of the transport microsteps, we have the function $\overline{\mathbf{S}}_n = \mathbf{z}_{n,i_2-1}(t_{n+1}) \in W$ that will serve as the initial condition at time t_n for the diffusive step. We shall apply backward differencing in time over $[t_n, t_{n+1}]$; i.e., we shall apply the mixed finite element method to the equations

$$\mathbf{V}_{n+1} = -KD\big(\overline{\mathbf{S}}_n\big)\left(\nabla \mathbf{S}_{n+1} + \frac{(\rho_{\mathrm{w}} - \rho_{\mathrm{o}})g\nabla z}{P_{\mathrm{c}}'(\overline{\mathbf{S}}_n)}\right), \tag{8.1a}$$

$$\Phi\frac{\mathbf{S}_{n+1} - \overline{\mathbf{S}}_n}{\Delta t_{\mathrm{s}}} + \operatorname{div}\mathbf{V}_{n+1} = 0, \tag{8.1b}$$

subject to the boundary condition

$$\mathbf{V}_{n+1} \cdot \vec{n} = 0. \tag{8.2}$$

Thus, the mixed finite element equations take the form

$$\left(\frac{1}{KD(\overline{\mathbf{S}}_n)}V_{n+1}, \vec{v}\right) - \big(\mathbf{S}_{n+1}, \operatorname{div}\vec{v}\big) = -\left(\frac{1}{P_{\mathrm{c}}'(\overline{\mathbf{S}}_n)}(\rho_{\mathrm{w}} - \rho_{\mathrm{o}})g\nabla z, \vec{v}\right), \quad \vec{v} \in \mathcal{V}, \tag{8.3a}$$

$$\left(\Phi\frac{\mathbf{S}_{n+1} - \overline{\mathbf{S}}_n}{\Delta t_{\mathrm{s}}}, w\right) + (\operatorname{div}\mathbf{V}_{n+1}, w) = 0, \qquad w \in W. \tag{8.3b}$$

9. The LCELM pressure calculation

Assume that $\mathbf{S}^m$ has been computed through the fractional step procedure outlined in the previous two sections. Then, the equations for $(\mathbf{U}^m, \mathbf{P}^m)$ are given by (see (6.1a)–(6.1b))

$$\mathbf{U}^m = -K\Lambda\big(\mathbf{S}^m\big)\big(\nabla\mathbf{P}^m - \big(\Lambda_{\mathrm{w}}\big(\mathbf{S}^m\big)\rho_{\mathrm{w}} + \Lambda_{\mathrm{o}}\big(\mathbf{S}^m\big)\rho_{\mathrm{o}}\big)g\nabla z\big), \tag{9.1a}$$

$$\operatorname{div}\mathbf{U}^m = q, \tag{9.1b}$$

subject to the boundary condition $\mathbf{U}^m \cdot \vec{n} = 0$ on $\partial\Omega$. The corresponding mixed finite

element equations are

$$\left(\frac{1}{K\Lambda(\mathbf{S}^m)}\mathbf{U}^m, \vec{v}\right) - \left(\mathbf{P}^m, \operatorname{div}\vec{v}\right)$$
$$= \left(\left(\Lambda_{\mathrm{w}}\left(\mathbf{S}^m\right)\rho_{\mathrm{w}} + \Lambda_{\mathrm{o}}\left(\mathbf{S}^m\right)\rho_{\mathrm{o}}\right)g\nabla z, \vec{v}\right), \quad \vec{v} \in \mathcal{V}, \tag{9.2a}$$
$$\left(\operatorname{div}\mathbf{U}^m, w\right) = (q, w), \qquad w \in W. \tag{9.2b}$$

10. Implementation

Much of the implementation of the LCELM code for the waterflood problem was taken directly from the code for the MMOCAA approximation of the same problem described in [23]. Since the transport step for the saturation is completely different from that used in the MMOC and MMOCAA procedures, its implementation will be described in reasonable detail below.

The transport microstep requires an exact evaluation of the integral of $\mathbf{\Phi z}_{n,\kappa}$ over $\overline{\mathbf{K}}_{ij}$. One algorithm for doing this for the rectangular partition of Ω is the following (with the time indices n, κ suppressed to simplify notation):

1. Given $\overline{\mathbf{K}}_{ij}$ as the quadrilateral with vertices $\overline{\mathbf{x}}_{ijk}$, $k = 1, \ldots, 4$, where the vertices are ordered in a counterclockwise fashion, determine $\{\alpha_k, \beta_k\}$ such that $\overline{\mathbf{x}}_{ijk} \in M_{\alpha_k,\beta_k}$ (see figure 2).

2. For the pairs $\{k, k+1\} = \{1,2\}, \ldots, \{4,1\}$, determine the intersections, in order, of the line segment $[\overline{\mathbf{x}}_{ijk}, \overline{\mathbf{x}}_{i,j,k+1}]$ with the element interfaces. Denote these points on $[\overline{\mathbf{x}}_{ijk}, \overline{\mathbf{x}}_{i,j,k+1}]$ by $\overline{\mathbf{y}}_{ijk\ell} = (x_{ijk\ell}, y_{ijk\ell})$, $\ell = 0, \ldots, L_{ijk}$, where $\overline{\mathbf{y}}_{i,j,k,0} = \overline{\mathbf{x}}_{ijk}$ and $\overline{\mathbf{y}}_{i,j,k,L_{ijk}} = \overline{\mathbf{x}}_{i,j,k+1}$.

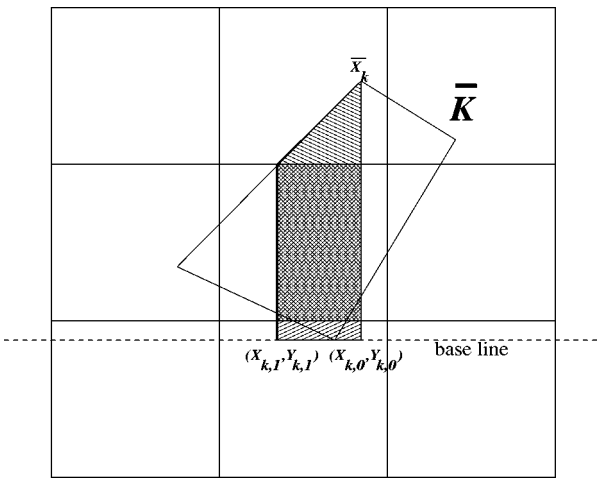

Figure 2. Exact calculation of water content on $\overline{\mathbf{K}}_{ij}$.

3. Determine a base line $\{y = y^*\}$, where $y^* = \min\{y\colon\ (x, y) \in \overline{\mathbf{K}}_{ij}\}$.

4. For each segment $[\overline{\mathbf{x}}_{ijk}, \overline{\mathbf{x}}_{i,j,k+1}]$, compute the integral $Q_{ijk\ell}$, $\ell = 1, \ldots, L_{ijk}$, of $\mathbf{\Phi z}_{n,\kappa}$ over the quadrilateral having base $[(x_{i,j,k,\ell-1}, y^*), (x_{ijk\ell}, y^*)]$ and top $[\overline{\mathbf{y}}_{i,j,k,\ell-1}, \overline{\mathbf{y}}_{ijk\ell}]$. Since $\mathbf{\Phi z}_{n,\kappa}$ is constant on elements, this integral can be broken into integrals over at most one triangle and a few rectangles on which the integrand is constant. Sum for $\ell = 1, \ldots, L_{ijk}$:

$$Q_{ijk} = -\text{sign}(x_{i,j,k,L_{ijk}} - x_{i,j,k,0}) \sum_{\ell=1}^{L_{ijk}} Q_{ijk\ell}.$$

5. Set

$$\int_{\overline{\mathbf{K}}_{ij}} \mathbf{\Phi z}_{n,\kappa}\, \mathrm{d}x = \sum_{k=1}^{4} Q_{ijk}. \tag{10.1}$$

The integrals involving the external flow rate are usually trivial in the waterflood problem, since the sources and sinks are normally considered as Dirac measures; if they are considered to be distributed, an algorithm analogous to the one above can be invoked.

It is not difficult to construct a corresponding algorithm for a simplicial partition of $\mathbf{\Omega}$, but we shall not do so here.

The diffusive part of the saturation calculation is very similar to that described in complete detail in [23]; the only difference is in the definition of the saturation flux V. Its definition in this paper leads to a simpler procedure in the presence of gravity terms. Otherwise, the implementation can be based on hybridizing [5] the mixed method by introducing Lagrange multipliers for the saturation on the faces of the elements and applying a standard quadrature based on the vertices before introducing a domain decomposition iteration based on Robin transmission conditions to solve the algebraic equations. This technique is explained in [23].

The pressure calculation in the code used to produce the examples in this paper is somewhat different from what was described in [23]. The mixed method equations are reduced to cell-centered finite differences as usual (and as in [23]) by hybridization, quadrature, and elimination of the flux variables and Lagrange multipliers; then, here, we apply a preconditioned conjugate gradient iteration in place of the domain decomposition iteration of [23]. We employed SSOR as the preconditioner.

11. Numerical experiments

We present some numerical results in this section to show some of the advantages of the LCELM in comparison with the MMOC and the MMOCAA. Three different reservoir geometries will be considered: a horizontal slab, a horizontal five-spot pattern, and a vertical cross-section.

Unless otherwise noted, the boundary conditions and injection and production specifications are as follows. For the horizontal slab, injection is made uniformly along the left edge of the reservoir and the (total) production rate is taken to be uniform along the right edge; no flow is allowed along the edges appearing at the top and bottom of the reservoir in the graphics. In the case of a five-spot flood, injection takes place at one corner and production at the diametrically opposite corner; no flow is allowed across the entirety of the boundary. (These specifications, if applied to inhomogeneous reservoirs, would represent somewhat nonphysical boundary conditions. As a result, we do not include any five-spot, inhomogeneous media experiments.) For vertical cross-sections, injection is usually specified at the lower left corner of the reservoir and production at the upper right corner; flow is prohibited across the entire boundary. For the horizontal slab and vertical cross-section examples, the conditions above will be applied to both homogeneous and inhomogeneous reservoirs.

The following data and functions are held fixed for the computational results:

Viscosity:	$\mu_{\mathrm{w}} = 0.5$ cP,	$\mu_{\mathrm{o}} = 10$ cP.
Density:	$\rho_{\mathrm{w}} = 1$ g/cm^3,	$\rho_{\mathrm{o}} = 0.7$ g/cm^3.
Porosity:	$\Phi = 0.2$.	
Residual saturations:	$S_{\mathrm{rw}} = 0.2$,	$S_{\mathrm{ro}} = 0.15$.
Absolute permeability:	$K = 6$ mdarcy.	
Relative permeability:	$K_{\mathrm{rw}}(S) = \dfrac{(S - S_{\mathrm{rw}})^2}{(1 - S_{\mathrm{rw}})^2}$,	$K_{\mathrm{ro}}(S) = \left(1 - \dfrac{S}{(1 - S_{\mathrm{ro}})}\right)^2$.
Capillary pressure:	$P_{\mathrm{c}}(S) = \eta\left(\dfrac{1}{(S - S_{\mathrm{rw}})^2} - \dfrac{\zeta}{(1 - S)^2}\right)$,	
	$\zeta = S_{\mathrm{ro}}^2(1 - S_{\mathrm{ro}} - S_{\mathrm{rw}})^{-2}$,	$\eta = 3000$ dynes /cm^2.

Initially, each reservoir is assumed to be in capillary and gravitational equilibrium. Thus, the initial condition for the system can be obtained as follows. Assume $\Psi_{\mathrm{w}} = 0$ and $\Psi_{\mathrm{o}} = C_\psi$ for some constant C_ψ. The water saturation in the reservoir can be computed using the capillary pressure function. Since different values of C_ψ correspond to different total fractions of water inside the reservoir, it is easy to find a C_ψ corresponding to a given fraction of water in the reservoir by, for example, binary search. Horizontal slab reservoirs are assumed to have dimension 256×64 meters; five-spot reservoirs are assumed to be 256×256 meters; and vertical cross-section reservoirs are 256×24 meters. Unless indicated otherwise, the injection rate is one pore-volume of water every five years. In the experiments on horizontal reservoirs, the initial water saturation was fixed uniformly at 0.21.

Some simulations reported use heterogeneous, multiscale, fractal, lognormal permeability fields. See [22,34,35] for a discussion of the numerical construction and the use of such fields in modelling stochastic geology and [23,27] for their use in MMOCAA calculations. In the case of heterogeneous permeability fields, the effect on the flow caused by the variations in permeability is investigated. We shall see a much greater difference between the flow patterns predicted by the three numerical methods than for homogeneous permeability. In particular, a more detailed picture of

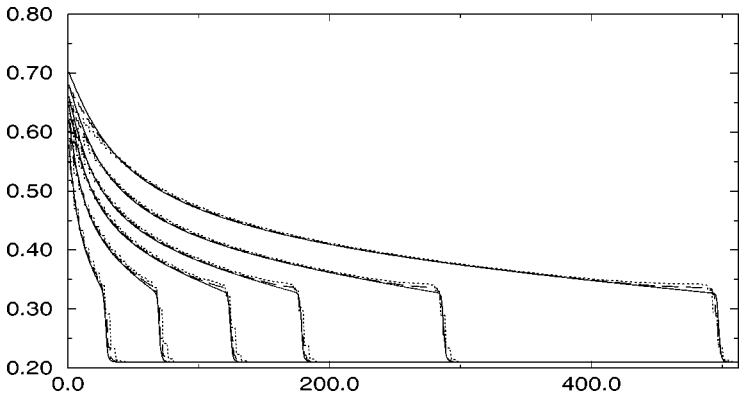

Figure 3. Grid refinement study for a homogeneous linear waterflood as approximated by an LCELM calculation. Three grids: $H = 2, 1, 0.5$ meters. Results shown at 20, 50, 90, 130, 210, 365 days.

the local behavior of the saturation will result from the LCELM calculations than can be obtained for similar levels of spatial and temporal discretization for the other two methods. A dimensionless parameter which measures the variability of the field is given by the coefficient of variation

$$C_{\mathrm{v}} = \sigma_K \Big/ \left(\frac{1}{|\Omega|} \int_\Omega K(x)\,\mathrm{d}x \right),$$

the ratio of the standard deviation of K to its mean value. In the experiments, C_{v} will be specified at the proper place. In each flood considered here, the permeability field is given by

$$K = K_{\mathrm{a}} \mathrm{e}^{\mathcal{S}\xi(x)},$$

where the average permeability K_{a} is 6 md for all floods, $\xi(x)$ a (mean 0) Gaussian random field, and $\mathcal{S}$ the strength of the heterogeneity of the field; increasing $\mathcal{S}$ increases C_{v}.

11.1. Justification of the algorithm and numerical convergence studies

The first set of simulations consists of a grid refinement study for flooding a homogeneous, horizontal, one-dimensional reservoir of length 256 meters; the spatial discretizations used corresponded to H equal to 2 meters, 1 meter, and 0.5 meters. Figure 3 shows a very satisfactory convergence of the numerical solutions for the water saturation S as computed by the LCELM technique for the three choices of H.

We now turn to an LCELM mesh refinement study for a homogeneous vertical cross-section flood simulated at 60 and 180 days. Figure 4 shows saturation level curves; the computational grids were 128×24 (top picture), 256×48 (middle picture),

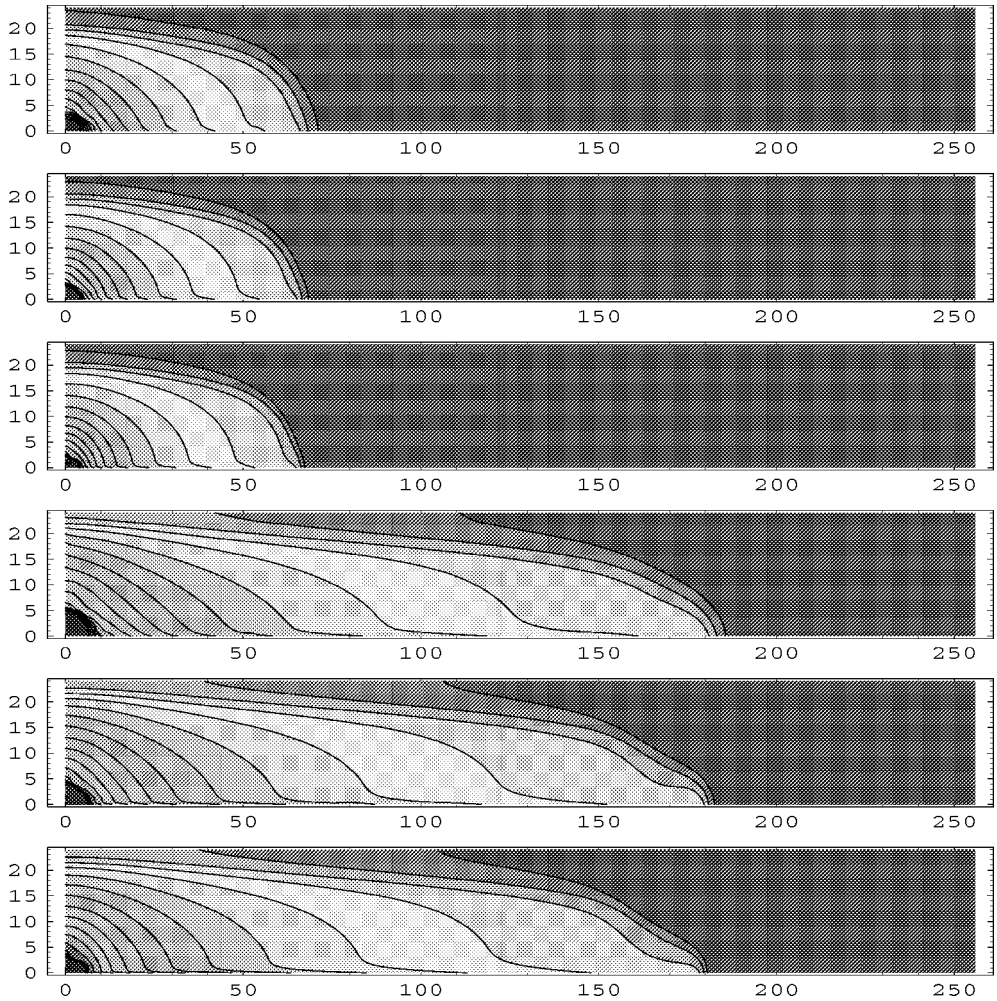

Figure 4. Mesh refinement study for a homogeneous vertical cross-section flood as simulated by the LCELM at 60 and 180 days. The grids used were 128×24 (top picture in each triple), 256×48 (middle picture), and 512×96 (bottom picture).

and 512×96 (bottom picture). The relative error measured in terms of the L_1 norm is given by

$$E_b^a = \int |f_a - f_b| \, \mathrm{d}x \Big/ \int |f_b| \, \mathrm{d}x,$$

where a and b specify the computational grids involved in the error computation. For this experiment,

$$E_{512}^{128} = 0.01132 \quad \text{and} \quad E_{512}^{256} = 0.00404 \quad \text{at 60 days,}$$
$$E_{512}^{128} = 0.01893 \quad \text{and} \quad E_{512}^{256} = 0.00711 \quad \text{at 180 days.}$$

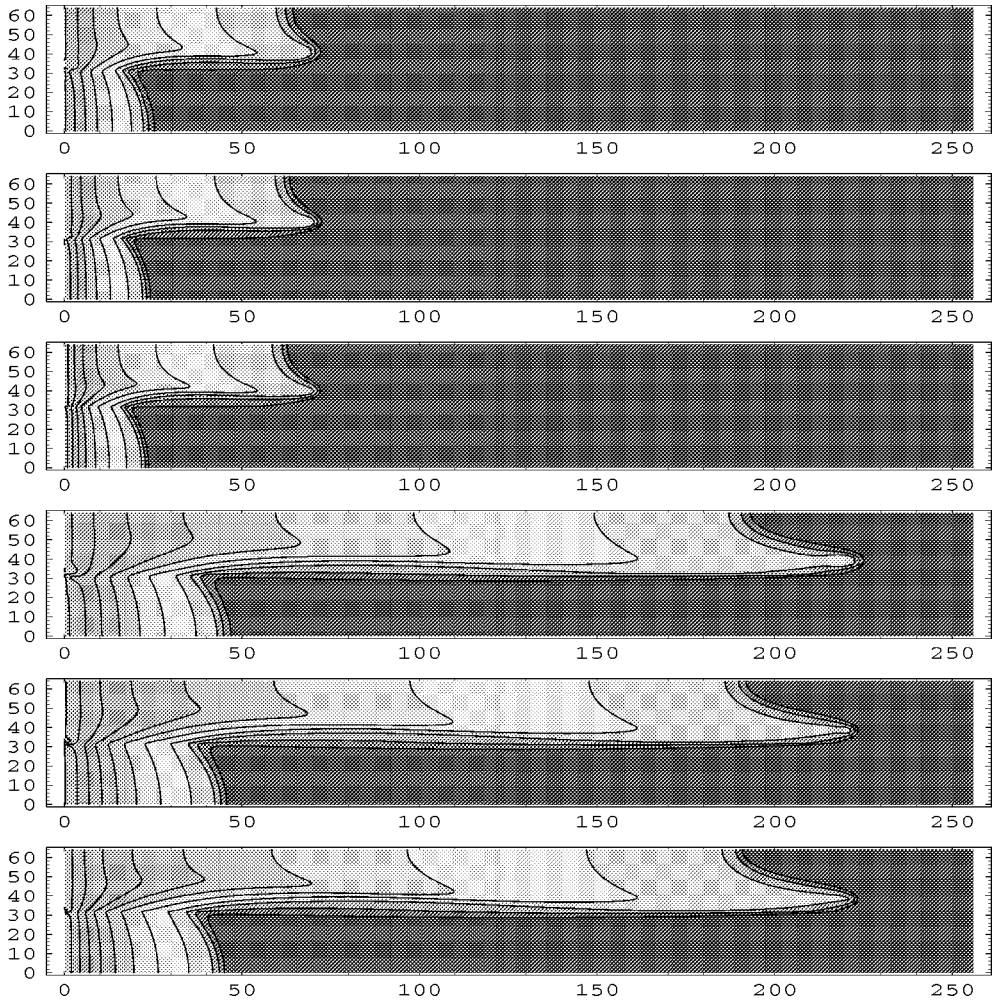

Figure 5. Mesh refinement study at 60 and 180 days for a horizontal slab. The absolute permeability is 6 md in the bottom half and 30 md in the top half. The L_1 norms with respect to the finest discretization considered are $E_{512}^{128} = 0.00942$ and $E_{512}^{256} = 0.00401$ at 60 days and $E_{512}^{128} = 0.01314$ and $E_{512}^{256} = 0.00534$ at 180 days.

Next, we considered a mesh refinement study for a horizontal slab having dimension 256×64 meters. The absolute permeability for the top half is 30 md and that of the bottom half is 6 md. Figure 5 displays saturation level curves at 60 and 180 days. The relative errors computed with respect to the finest discretization considered in figure 5 are $E_{512}^{128} = 0.01314$ and $E_{512}^{256} = 0.00534$ at 180 days, clearly indicating a satisfactory numerical convergence of the procedure.

Figures 6 and 7 present mesh refinement studies for two vertical cross-section floods, one with a lower permeability in the top half of the reservoir than in the bottom half and the second with the permeabilities interchanged; the ratio of the two

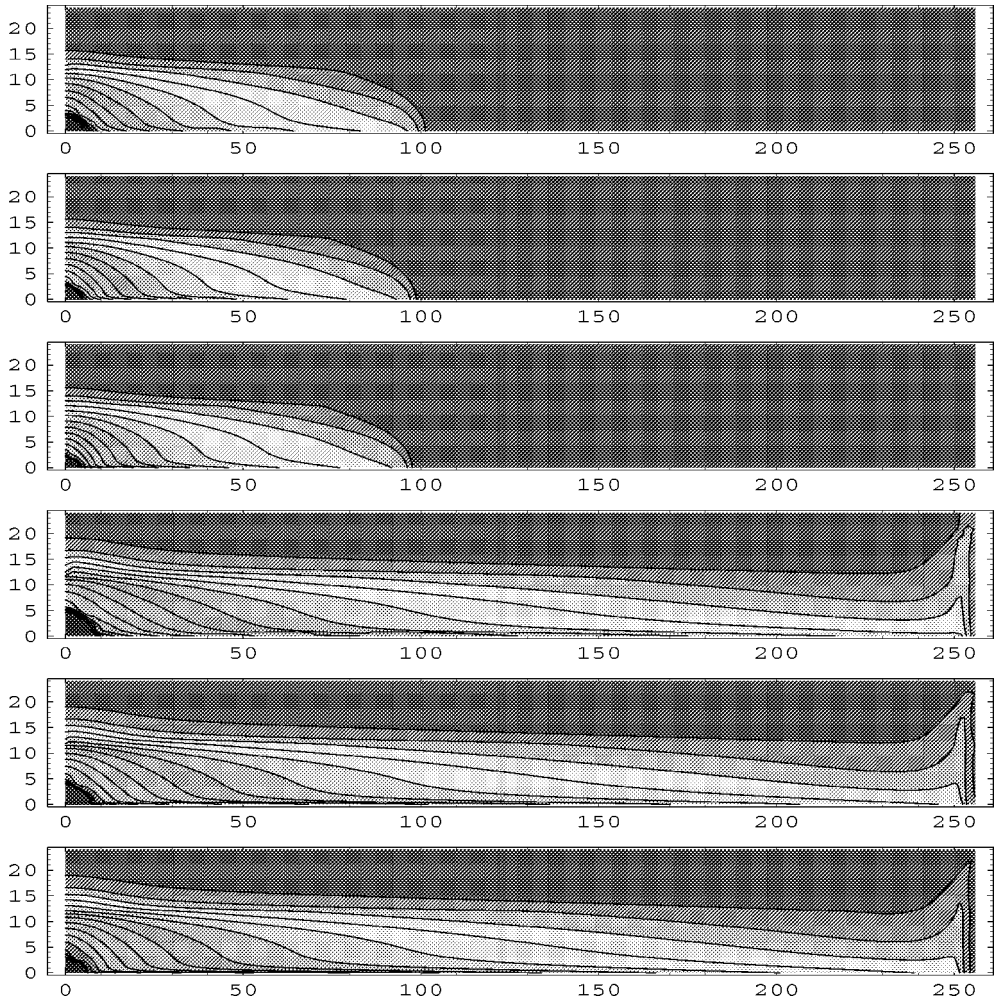

Figure 6. Mesh refinement study at 60 and 180 days for a vertical cross-section; $H = 2$ m, 1 m, and 0.5 m. The absolute permeability is 30 md in the bottom half and 6 md in the top half. The L_1 norms with respect to the finest discretization considered are $E_{512}^{128} = 0.02109$ and $E_{512}^{256} = 0.00862$ at 180 days.

permeabilities is 5 in each case. Note that breakthrough at the outflow well has occurred at 180 days in the case that the higher permeability was on the bottom, but not when the lower permeability was on the bottom. Breakthrough had not yet occurred for a uniform permeability (figure 4).

The next figure, figure 8, presents permeability fields on 16×16 and 64×64 grids; the 16×16 field is employed in a mesh refinement study aimed at showing the superiority of one method of evaluating the Darcy velocity in the construction of the predecessor set $\overline{K}$ for an element K over another evaluation. The 64×64 grid is used in a study of the relation between the permeability grid and the computational grid.

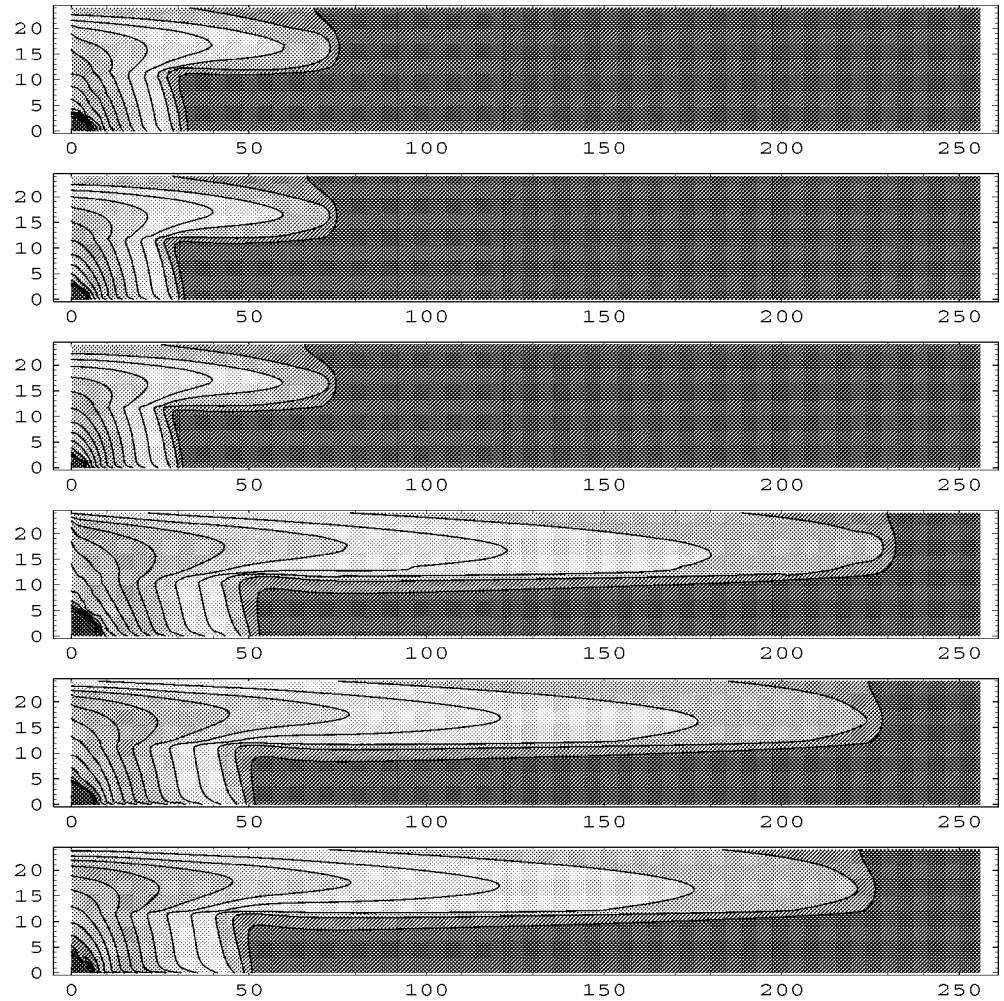

Figure 7. Mesh refinement study at 60 and 180 days for a vertical cross-section; $H = 2$ m, 1 m, and 0.5 m. The absolute permeability is 6 md in the bottom half and 30 md in the top half. The L_1 norms with respect to the finest discretization considered are $E_{512}^{128} = 0.01134$ and $E_{512}^{256} = 0.00397$ at 180 days.

We defined the predecessor set $\overline{K}$ for K tracing back the tangents to the integral curves at the vertices of K to the previous (micro)time level. Recall that the Darcy velocity U has been approximated by a Raviart–Thomas mixed method; thus, it is not uniquely defined at a vertex of an element. As previously noted, the simplest evaluation of it at a vertex is obtained by averaging the two values of the x-component at the midpoints of the vertical (in figure 8) faces of the four elements abutting the vertex and averaging the corresponding y-components. The three individual pictures in the left column of figure 9 present a mesh refinement study based on this evaluation; the result is that refinement leads to increased, spurious local oscillation of the approximate saturation. The second method of evaluating U at a vertex is based on bilinearly

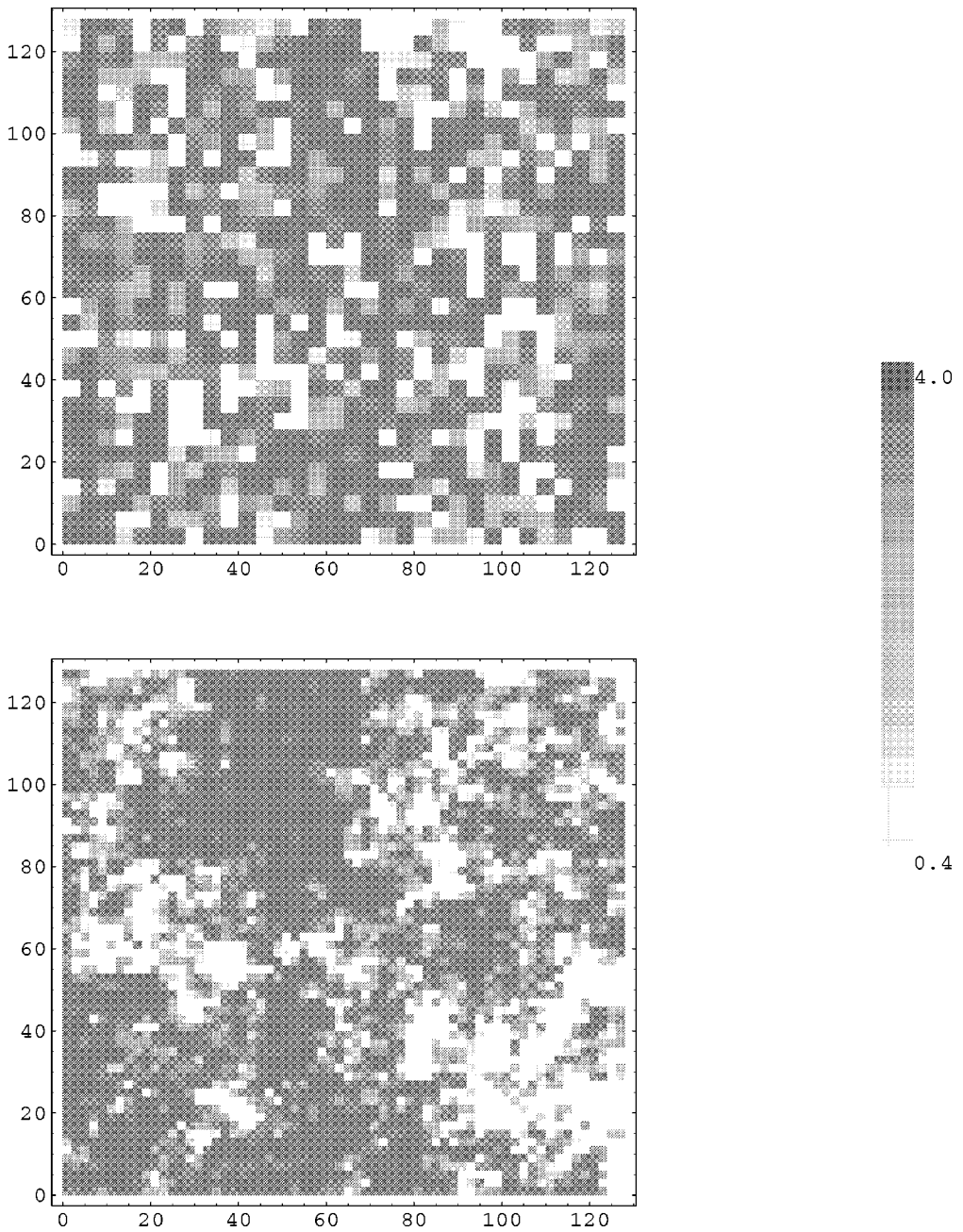

Figure 8. Coarse grid permeability fields used in the simulations reported in figures 9 (top field) and 10 (bottom field). The fields are piecewise constant on a 16×16 grid (top picture) and on a 64×64 grid (bottom picture). Both fields are defined on a square of size 128×128 meters.

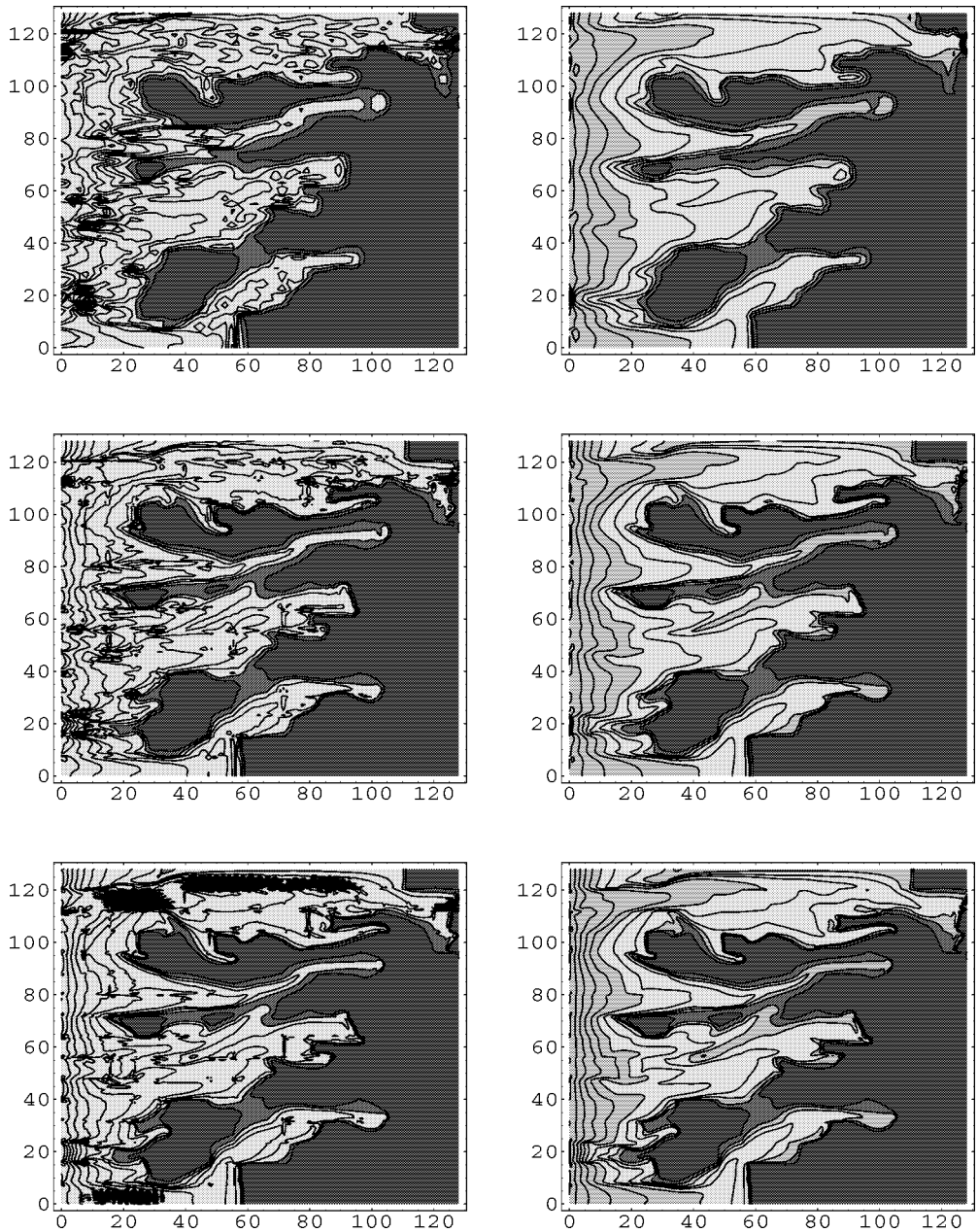

Figure 9. Mesh refinement study when U (global flux) components are computed by arithmetic averages (left column) and by bilinear interpolation (right column). From top to bottom the corresponding grid sizes are 64×64, 128×128, and 256×256.

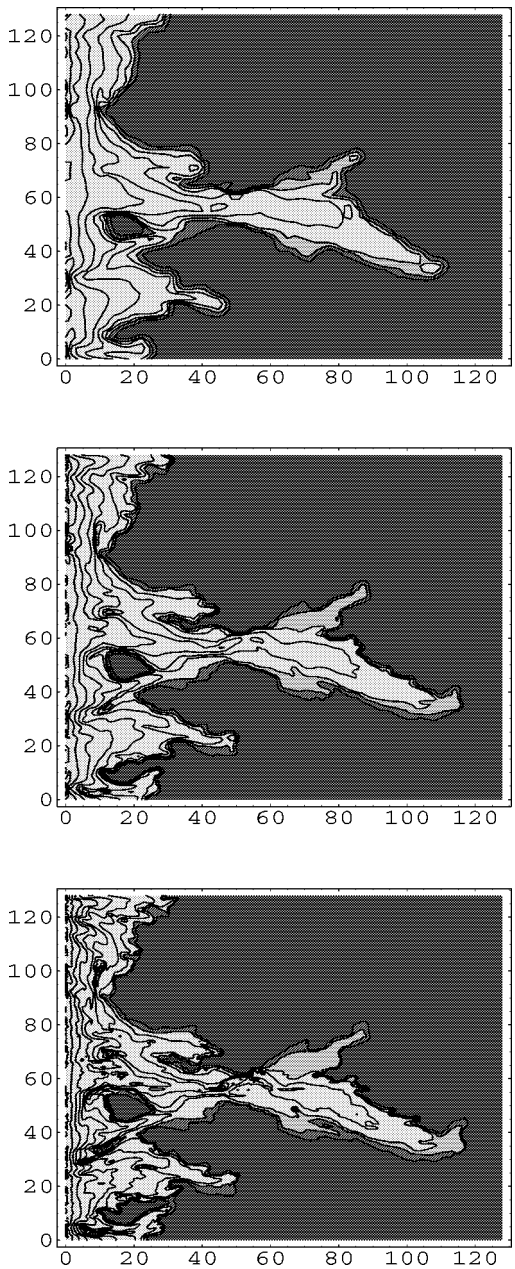

Figure 10. Mesh refinement study for a fractal permeability. The mesh size of the coarser grid (top) coincides with the size of the permeability grid block. The successive refinements refer to grids where the permeability grid blocks are divided into 4 (middle) and 16 (bottom) computational grid blocks.

interpolating the element-center values of the Raviart–Thomas approximation of U. The three pictures in the right column of figure 9 represent the corresponding mesh refinement study for this choice; note that no spurious oscillations appear and that there appears to be very little difference in the saturation profiles between the 128×128 computation and that for the 256×256 grid, and there is not much change between the 64×64 and 128×128 calculations.

Figure 10 presents a similar mesh refinement study when the permeability is given on a 64×64 grid. Here (and for all other simulations reported, except in the previous experiment), only the bilinearly interpolated U was employed. No spurious oscillations are observable, and the convergence of the approximate saturation is apparent.

We offer the following conjecture to explain the superior performance of the bilinearly interpolated U. Away from sources and sinks (i.e., almost everywhere in our examples), the bilinearly interpolated U is divergence-free in the neighborhood

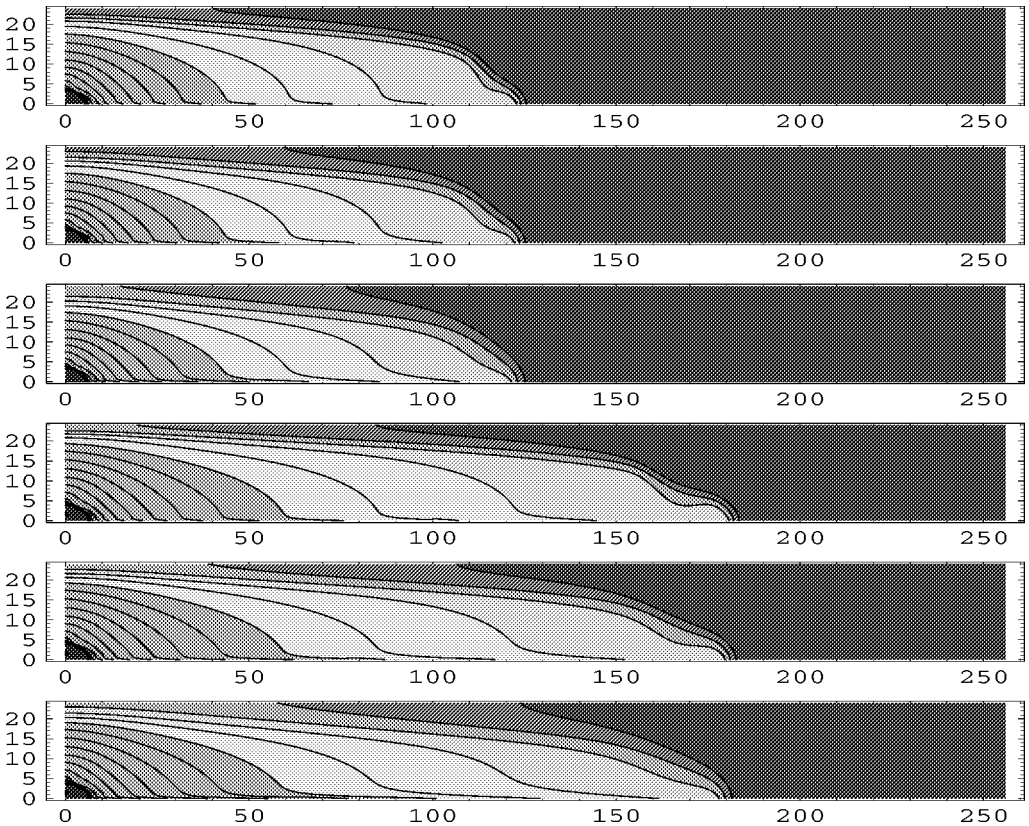

Figure 11. Comparison of LCELM simulations of homogeneous vertical cross-section floods for injection rates of one pore volume every 2.5, 5, and 10 years. The results are for 120 days (top three pictures) and 180 days (bottom three pictures) using a 256×48 grid. In each triple, the upper contour profile corresponds to the fastest rate, the middle one to the intermediate rate, and the lowest one to the slowest rate.

of vertices; the simpler procedure induces some divergence about the vertices. We suspect that these small divergences are responsible for the local oscillations. If our conjecture is correct, then spurious oscillations come from an inadequate interpretation of the results of the pressure calculations.

Figure 11 presents saturation profiles as computed by the LCELM in a vertical cross-section flood with three different injection rates but at the same total pore volumes injected. The top picture represents injection of one pore volume of water every 2.5 years, while the middle picture corresponds to one pore volume every five years and the bottom picture to an injection rate of one pore volume every 10 years. Injection takes place at the lower left corner and production at the upper right corner. The figure shows that slower injection produces a more efficient sweeping out of the oil, as corresponds to decades of experience.

11.2. Comparisons between MMOC, MMOCAA, and LCELM simulations

We first compare results obtained by the MMOC, MMOCAA, and LCELM techniques for homogeneous reservoirs with the three geometries specified above. It will be seen that, as expected, the MMOC loses mass in all of these experiments. The viscous fingers computed by the LCELM move faster and have sharper tips than those obtained by the other two methods. A possible explanation for the increased sharpness at the tips of fingers is that transport is computed in an almost exact fashion without the interpolation of the saturation at the previous time level required by the characteristic methods in the evaluation of the saturation at the feet of the characteristics.

Figure 12 is a comparison of the water saturation obtained through the MMOC, MMOCAA, and LCELM procedures for the homogeneous linear waterflood problem at several times; $H = 1$ meter in all three runs. The MMOC loses mass, which leads to the front being delayed. The front for the LCELM moves faster and is sharper than those for the other two, even though the MMOCAA maintains the same quantity of

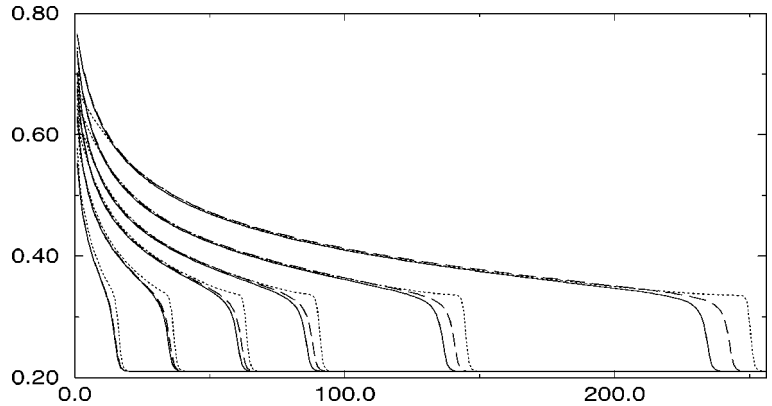

Figure 12. Comparison of MMOC, MMOCAA, and LCELM simulations of a homogeneous linear waterflood at 20, 50, 90, 130, 210, 365 days. The solid curves correspond to the MMOC, the dashed to the MMOCAA, and the dotted to the LCMMOC.

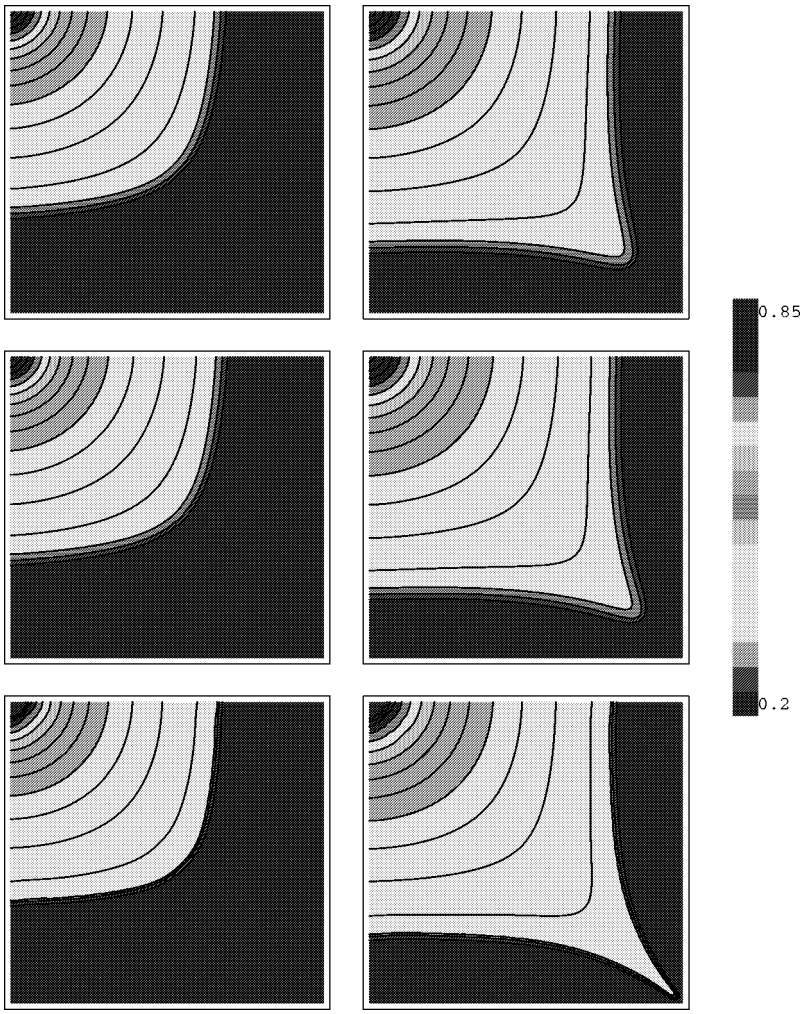

Figure 13. Approximation of a homogeneous five-spot flood by MMOC (top), MMOCAA (middle), and LCELM (bottom) calculations at 140 (left) and 230 (right) days using a 128×128 grid.

water inside the reservoir as the LCELM, at least until the water breaks through at the outflow face.

Figure 13 gives a comparison of saturation contours for a five-spot flood for the MMOC, MMOCAA, and LCELM procedures at 140 and 230 days injected. Water is injected into the reservoir at the top left corner at a uniform rate and a mixture of water and oil produced at the lower right corner. Again, water is lost by the MMOC calculation and the finger is sharper for the LCELM run than for the MMOCAA run, confirming the observations made concerning the linear waterflood.

Figure 14 presents the evolution of the saturation in a vertical cross-section flood resulting from injection at a uniform rate into the reservoir at the lower left corner and

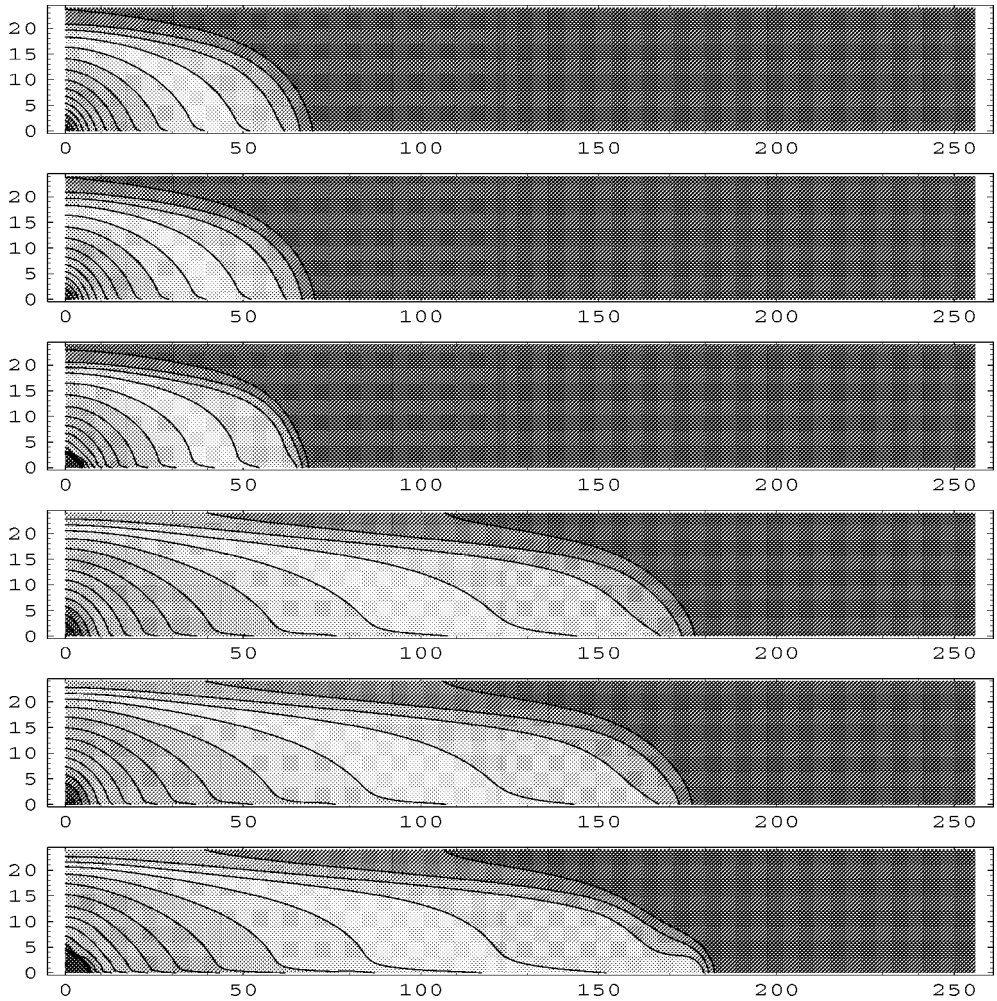

Figure 14. Approximation of a homogeneous vertical cross-section flood by MMOC (upper picture in each triple), MMOCAA (middle), and LCELM (lower) simulations at 60 and 180 days using a 256×48 grid.

a mixture of water and oil is produced at the upper right corner; gravitational effects are considered. As should be expected, gravity drives the water to run under the oil. There is less difference in the saturation level curves between the three procedures for this example than for any other that was run.

Next, we consider simulations in heterogeneous reservoirs. In this study, the effect on the flow of variations in the permeability fields is investigated. For the following three floods, the underlying Gaussian field $\xi(x)$ is indicated in figure 15 and the actual lognormal fields are pictured in figure 16. The two fields have identical regions of high and low permeabilities, but the field with the higher C_{v} has a much higher ratio between high values and low values.

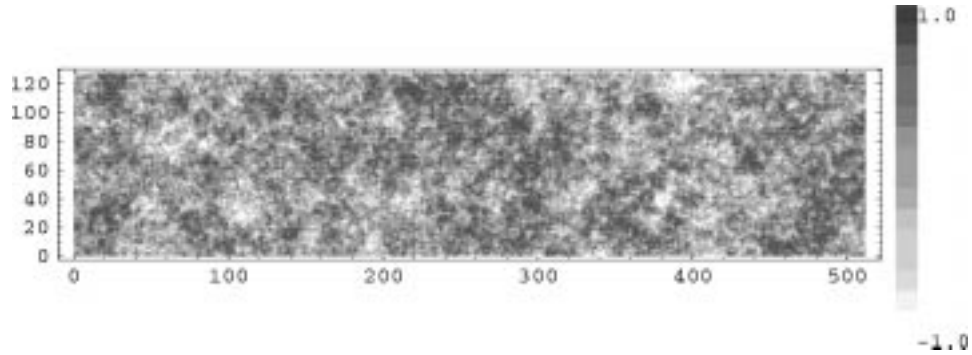

Figure 15. Underlying (mean zero) Gaussian field $\xi(x)$ for the construction of the permeability fields used in the next three floods.

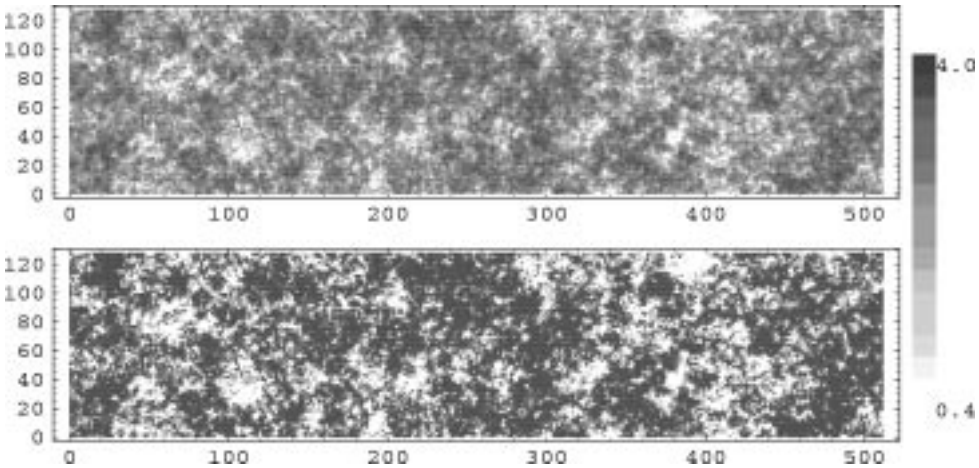

Figure 16. C_{v} study: the actual permeability fields with C_{v}-values 0.49 and 5.2 are in the top and bottom pictures.

The next two figures, figures 17 and 18, show saturation contours at 200 days. The loss of water in figure 17, where $\mathcal{S} = 1$ and $C_{\mathrm{v}} = 0.49$, for the standard MMOC is very significantly less than in figure 18, where $\mathcal{S} = 3.7$ and $C_{\mathrm{v}} = 5.2$ and 30% of the injected water has been lost. The tip of the primary finger has not reached 160 meters in the MMOC calculation when $C_{\mathrm{v}} = 5.2$, whereas it has advanced to about 215 meters in the MMOCAA calculation and 230 meters in the LCELM calculation. For the lower C_{v}, the corresponding numbers are 155, 170, and 180 meters. The difference in local detail obtained by the MMOCAA and LCELM methods is quite apparent in the higher C_{v} flood. The distinction between the simulations in the high C_{v} case is very visible in the plots of figure 19. Note, particularly, the difference in the sharpness of the saturation fronts, in addition to the obvious loss of water in the MMOC simulation.

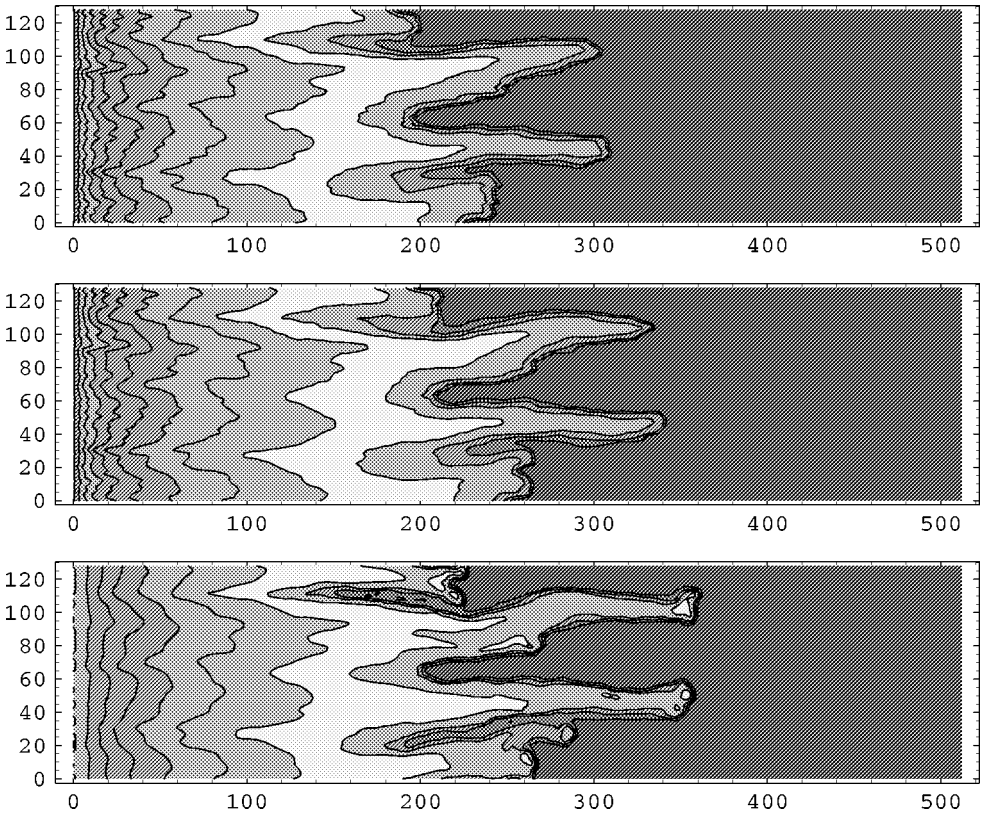

Figure 17. C_v study: horizontal slab flood at 200 days with $C_v = 0.49$. From top to bottom: MMOC, MMOCAA and LCELM.

For the next two studies, the C_v-values are 2.9 and 1.3, indicating a quite heterogeneous formation. The top two pictures in each study are related to the MMOC simulation, the third to the MMOCAA simulation, and the fourth to the LCELM simulation. The top MMOC picture reports the contours at the same computed time as for the contours for the MMOCAA and LCELM procedures. Recall that the MMOCAA is based on perturbing the feet of the characteristics involved in the MMOC each transport microstep in order to maintain a correct global mass balance at the end of every saturation time step. The lower MMOC picture represents a different approach to obtaining a global mass balance. To each computed time level for the MMOC simulation, associate a virtual time based on the mass of the water in place in the reservoir plus that which has been produced minus that which was initially in place; given the injection rate, this determines the virtual time. The lower MMOC picture reports the contours when the virtual time equals the computed time for the MMOCAA and LCELM simulations. Call the MMOC procedure, as modified by replacing the computed time by the virtual time, the VMMOC procedure. Then, the contours for the MMOCAA and the VMMOC calculations are almost identical. The first study,

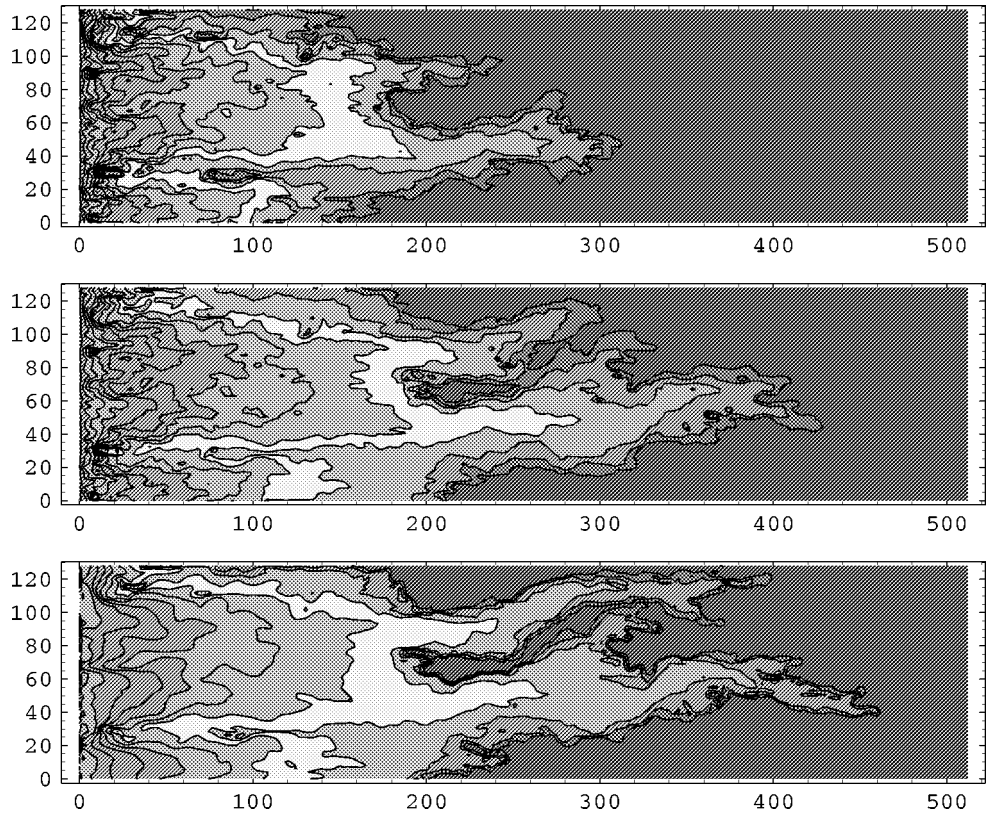

Figure 18. C_v study: horizontal slab flood at 200 days with $C_v = 5.2$. From top to bottom: MMOC, MMOCAA and LCELM.

figure 20, refers to a heterogeneous horizontal slab flood and the second, figure 21, to a vertical cross-section flood.

12. Miscible displacement

The standard (though not completely correct) model for miscible displacement (see [39]) for a mixture of a solvent with concentration C and oil in a gravity-free environment is given in divergence form by

$$\operatorname{div} U \equiv -\operatorname{div}\left(\frac{K}{\mu(C)}\nabla P\right) = q \quad \text{(pressure equation)}, \tag{12.1a}$$

$$\Phi\frac{\partial C}{\partial t} - \operatorname{div}(D\nabla C - CU) = \widetilde{C}q \quad \text{(concentration equation)}. \tag{12.1b}$$

Here, U is the volumetric convective flow rate of the mixture per unit cross-sectional area, $K = K(x)$ is the rock absolute permeability, $\mu = \mu(C)$ is the concentration-dependent fluid viscosity, P is the fluid pressure, $\Phi = \Phi(x)$ is the porosity of the

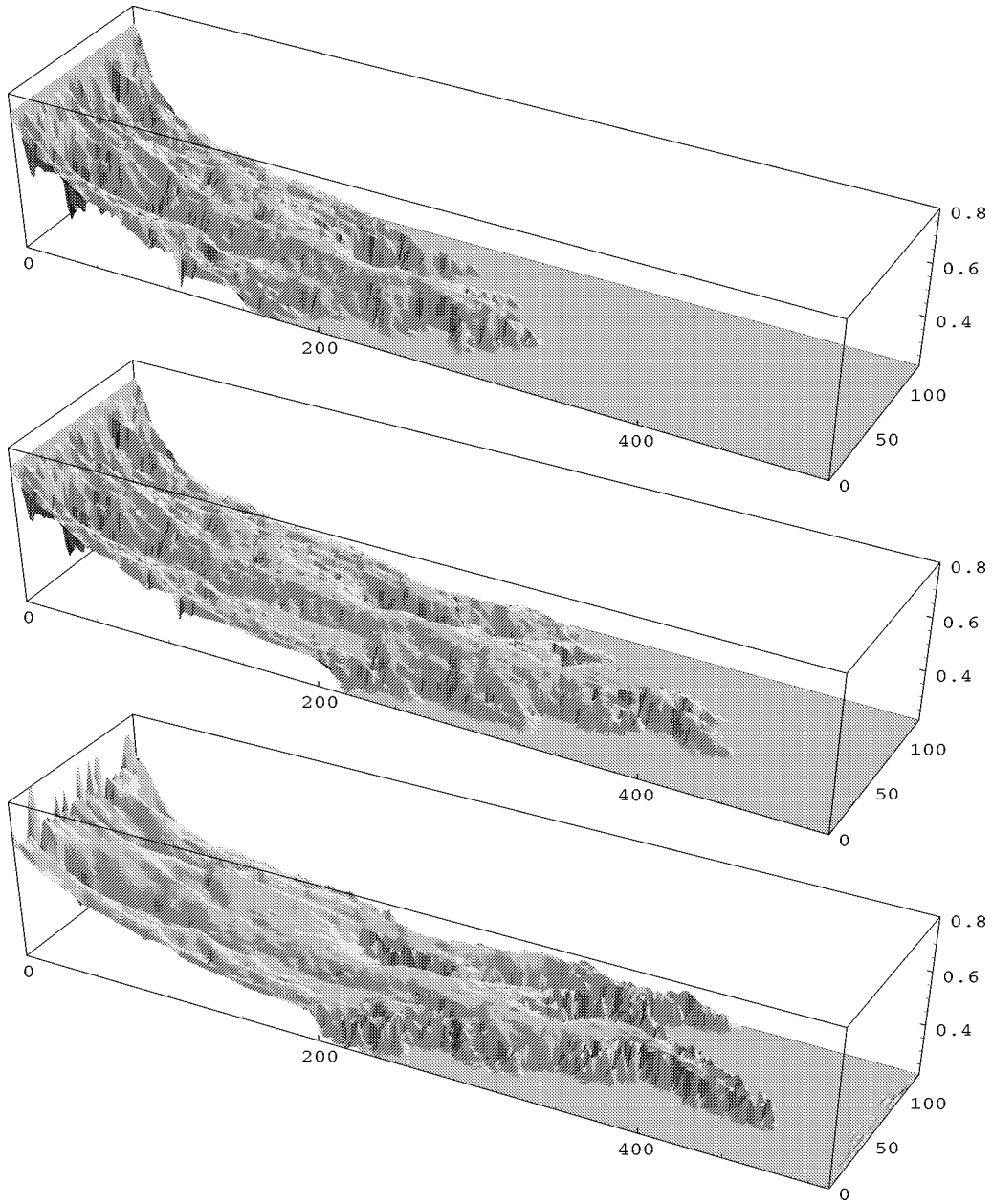

Figure 19. Saturation surface plots corresponding to the C_{v} study: horizontal slab flood at 200 days with $C_{\mathrm{v}} = 5.2$. From top to bottom: MMOC, MMOCAA and LCELM.

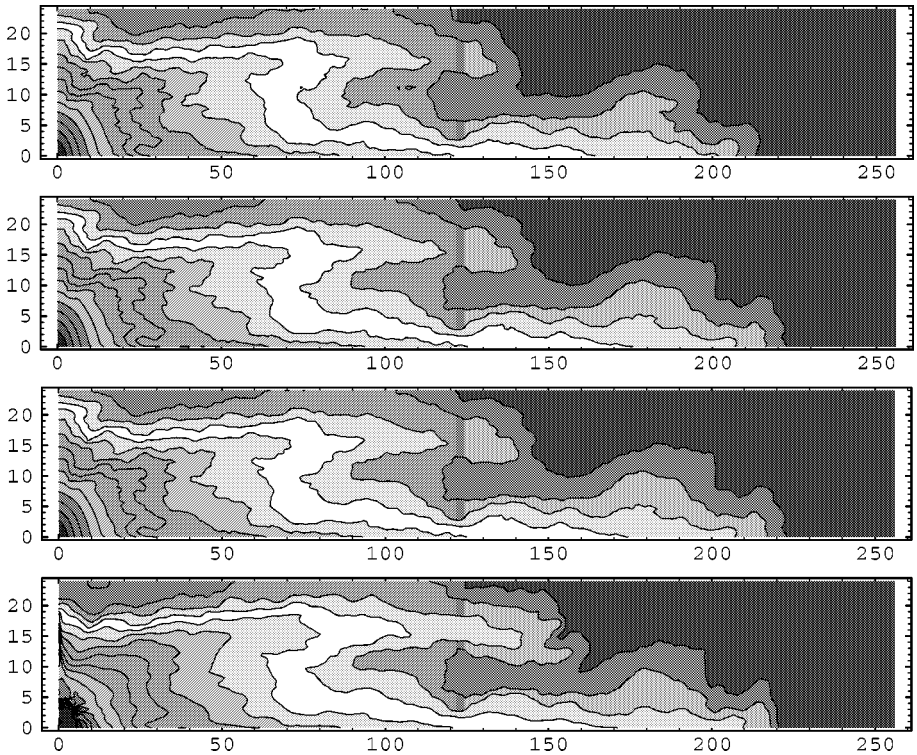

Figure 20. Comparison of MMOC, VMMOC, MMOCAA, and LCELM simulations of flooding a heterogeneous horizontal slab at 180 days; $C_{\mathrm{v}} = 2.9$ for the permeability field obtained from a different realization of the Gaussian field from the one shown in figure 15.

medium, q is the external volumetric flow rate per unit volume, $\widetilde{C}$ is the specified concentration of solvent at an injection well ($q > 0$) and the resident concentration at a production well ($q < 0$), and D is a diffusion–dispersion tensor given by

$$D = D(U) = \Phi d_m I + \frac{d_\ell}{|U|}\begin{pmatrix} U_x^2 & U_xU_y \\ U_xU_y & U_y^2 \end{pmatrix} + \frac{d_t}{|U|}\begin{pmatrix} U_y^2 & -U_xU_y \\ -U_xU_y & U_x^2 \end{pmatrix}.$$

The requisite boundary and initial conditions are specified by

$$U \cdot \vec{n} = 0, \qquad x \in \partial\Omega,\ t \in J; \tag{12.2a}$$

$$(D\nabla C - CU) \cdot \vec{n} = 0, \qquad x \in \partial\Omega,\ t \in J; \tag{12.2b}$$

$$C(x, 0) = C_0(x), \qquad x \in \Omega. \tag{12.2c}$$

Compatibility to incompressibility requires that

$$\int_\Omega q \,\mathrm{d}x = \int_\Omega \operatorname{div} U \,\mathrm{d}x = \int_{\partial\Omega} U \cdot \vec{n} \,\mathrm{d}s = 0. \tag{12.3}$$

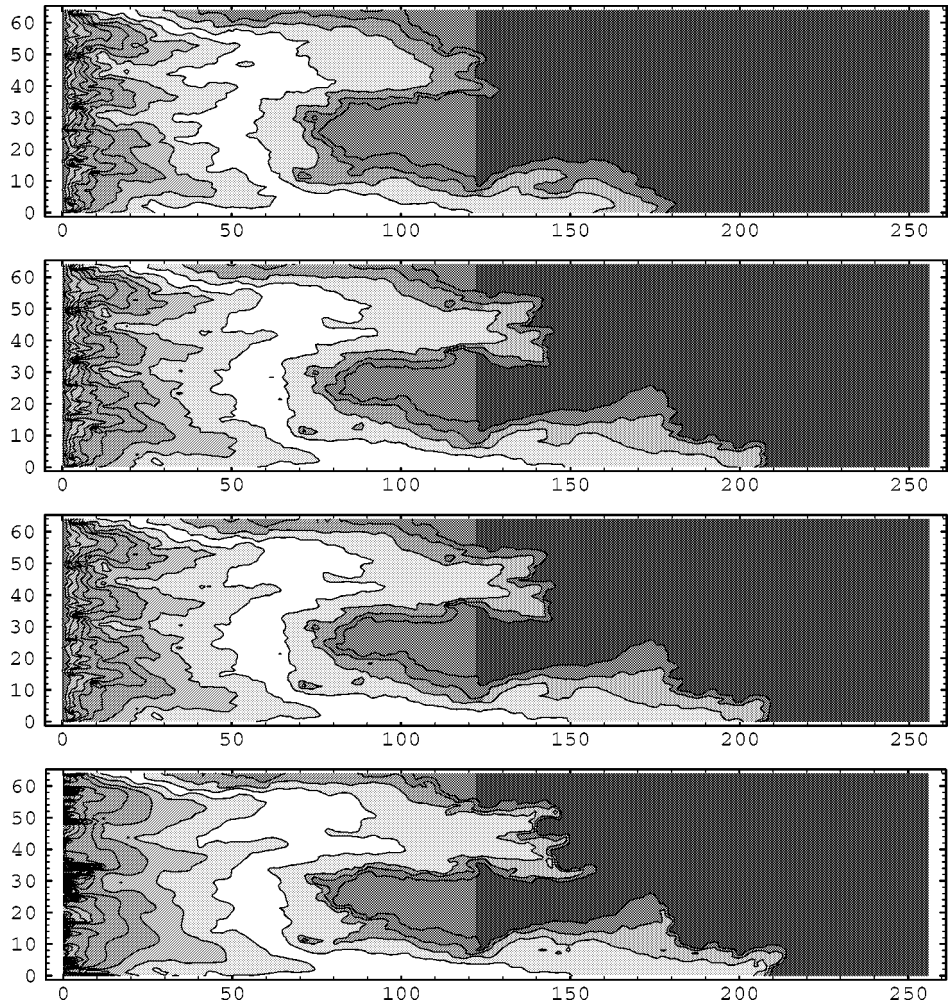

Figure 21. Comparison of MMOC, VMMOC, MMOCAA, and LCELM simulations of flooding a heterogeneous vertical cross-section at 180 days; $C_v = 1.3$ for the permeability field obtained from a different realization of the Gaussian field from the one shown in figure 15.

By (12.1a), $\operatorname{div}(CU) = U \cdot \nabla C + C(\operatorname{div} U) = U \cdot \nabla C + Cq$, and the concentration equation can be rewritten in nondivergence form as

$$\Phi \frac{\partial C}{\partial t} + U \cdot \nabla C - \operatorname{div}(D \nabla C) = \big(\widetilde{C} - C\big) q. \tag{12.4}$$

For any reasonable solvent injection rate, the flow is essentially along the characteristic associated with the transport $\Phi \partial C/\partial t + U \cdot \nabla C$, so that it is appropriate to introduce differentiation in this characteristic direction. Let

$$\Theta(x, U) = \big[\Phi(x)^2 + |U|^2\big]^{1/2}, \qquad \frac{\partial}{\partial \tau} = \frac{1}{\Theta}\left\{\Phi \frac{\partial}{\partial t} + U \cdot \nabla\right\}.$$

Then, the concentration equation can be rewritten yet again as

$$\Theta\frac{\partial C}{\partial \tau} - \operatorname{div}(D\nabla C) = \big(\widetilde{C} - C\big)q. \tag{12.5}$$

The direction τ depends on space and the fluid velocity, which varies in space and time.

Now, let us compare the integral curves $y(x;t)$ for (12.1b) given by

$$\frac{\mathrm{d}y}{\mathrm{d}t} = \frac{CU}{\Phi C} = \frac{U}{\Phi}, \qquad y(x, t_{n,\kappa+1}) = x, \tag{12.6}$$

and the characteristics for (12.4), which coincide with the integral curves above. Thus, the relation between the MMOC schemes and the LCELM procedure for miscible displacement is much closer than it was for immiscible displacement, since the tube **D** associated with a set **K** has its lateral surface determined by the same characteristics as are defined in the MMOC techniques. Note that the characteristics that would be used in the LCELM approach would be associated with vertices of **K**, rather than quadrature points usually in the interior of **K**.

The application of the LCELM concept to this miscible displacement problem will be taken up elsewhere; see [1]. It should be remarked that the LCELM scheme for this problem is essentially identical to an extension of the basic method of Arbogast and Wheeler [4]; they applied a somewhat modified version of the procedure to the miscible problem in [3].

Acknowledgements

The authors wish to thank Professor Frederico Furtado for many discussions on Eulerian–Lagrangian schemes. Our locally conservative scheme grew out of these discussions. They would like also to thank Professor Todd Arbogast for bringing an oscillation in the preliminary computed results to their attention; see figure 9, where we illustrate one source of oscillations and a cure for them. The authors thank FAPERJ for support related to the research reported herein. Also, Professor Yeh wishes to thank the National Science Council of the Republic of China for support.

References

[1] C. Almeida, J. Douglas, Jr. and F. Pereira, From nonconservative to locally conservative Eulerian–Lagrangian methods for miscible displacement in heterogeneous formations, to appear.

[2] S.N. Antontsev, On the solvability of boundary value problems for degenerate two-phase porous flow equations, Dinamika Splošnoĭ Sredy 10 (1972) 28–53 (in Russian).

[3] T. Arbogast, A. Chilikapati and M.F. Wheeler, A characteristics-mixed finite element for contaminant transport and miscible displacement, in: *Computational Methods in Water Resources IX*, Vol. 1: *Numerical Methods in Water Resources*, eds. T.F. Russell et al. (Elsevier Applied Science, London, 1992), pp. 77–84.

[4] T. Arbogast and M.F. Wheeler, A characteristics-mixed finite element method for advection-dominated transport problems, SIAM J. Numer. Anal. 32 (1995) 404–424.
[5] D.N. Arnold and F. Brezzi, Mixed and nonconforming finite element methods: implementation, postprocessing and error estimates, RAIRO Modél. Math. Anal. Numér. 19 (1985) 7–32.
[6] J.B. Bell, C.N. Dawson and G.B. Shubin, An unsplit high-order Godunov scheme for scalar conservation laws in two dimensions, J. Comput. Phys. 75 (1988) 1–24.
[7] F. Brezzi, J. Douglas, Jr., R. Durán and M. Fortin, Mixed finite elements for second order elliptic problems in three variables, Numer. Math. 51 (1987) 237–250.
[8] F. Brezzi, J. Douglas, Jr., M. Fortin and L.D. Marini, Efficient rectangular mixed finite elements in two and three space variables, RAIRO Modél. Math. Anal. Numér. 21 (1987) 581–604.
[9] F. Brezzi, J. Douglas, Jr. and L.D. Marini, Two families of mixed finite elements for second order elliptic problems, Numer. Math. 47 (1985) 217–235.
[10] M.A. Celia, T.F. Russell, I. Herrera and R.E. Ewing, An Euler–Lagrangian localized adjoint method for the advection–diffusion equations, Adv. Water Resources 13 (1990) 187–206.
[11] G. Chavent, A new formulation of diphasic incompressible flows in porous media, in: *Applications of Methods of Functional Analysis to Problems in Mechanics*, Lecture Notes in Mathematics, Vol. 503, eds. P. Germain and B. Nayroles (Springer, Berlin/New York, 1976) pp. 258–270.
[12] G. Chavent and J. Jaffré, *Mathematical Models and Finite Elements for Reservoir Simulation* (North-Holland, Amsterdam, 1986).
[13] Z. Chen and J. Douglas, Jr., Prismatic mixed finite elements for second order elliptic problems, Calcolo 26 (1989) 135–148.
[14] A. Chilakapati, A characteristic-conservative model for Darcian advection, Adv. Water Resources 22 (1999) 597–609.
[15] H.K. Dahle, R.E. Ewing and T.F. Russell, Eulerian–Lagrangian localized adjoint methods for a nonlinear advection–diffusion equation, Comput. Methods Appl. Mech. Engrg. 122 (1995) 223–250.
[16] J. Douglas, Jr., Simulation of miscible displacement in porous media by a modified method of characteristics procedure, in: *Numerical Analysis*, Lecture Notes in Mathematics, Vol. 912 (Springer, Berlin, 1982).
[17] J. Douglas, Jr., Finite difference methods for two-phase incompressible flow in porous media, SIAM J. Numer. Anal. 20 (1983) 681–696.
[18] J. Douglas, Jr., Numerical methods for the flow of miscible fluids in porous media, in: *Numerical Methods in Coupled Systems*, eds. R.W. Lewis, P. Bettess and E. Hinton (Wiley, London, 1984) pp. 405–439.
[19] J. Douglas, Jr., Superconvergence in the pressure in the simulation of miscible displacement, SIAM J. Numer. Anal. 22 (1985) 962–969.
[20] J. Douglas, Jr., R.E. Ewing and M.F. Wheeler, The approximation of the pressure by a mixed method in the simulation of miscible displacement, RAIRO Anal. Numér. 17 (1983) 17–33.
[21] J. Douglas, Jr., R.E. Ewing and M.F. Wheeler, A time-discretization procedure for a mixed finite element approximation of miscible displacement in porous media, RAIRO Anal. Numér. 17 (1983) 249–265.
[22] J. Douglas, Jr., F. Furtado and F. Pereira, The statistical behavior of instabilities in immiscible displacement subject to fractal geology, in: *Mathematical Modelling of Flow Through Porous Media*, eds. A.P. Bourgeat, C. Carasso, S. Luckhaus and A. Mikelić (World Scientific, Singapore, 1995) pp. 115–137.
[23] J. Douglas, Jr., F. Furtado and F. Pereira, On the numerical simulation of waterflooding of heterogeneous petroleum reservoirs, Computational Geosciences 1 (1997) 155–190.
[24] J. Douglas, Jr., C.S. Huang and F. Pereira, The modified method of characteristics with adjusted advection for an immiscible displacement problem, in: *Advances in Computational Mathematics*, Lecture Notes in Pure and Applied Mathematics, Vol. 202, eds. Z. Chen, Y. Li, C.A. Micchelli and Y. Xu (Marcel Dekker, New York, 1999) pp. 53–73.

[25] J. Douglas, Jr., C.S. Huang and F. Pereira, The modified method of characteristics with adjusted advection, Numerische Mathematik 83 (1999) 353–369.
[26] J. Douglas, Jr., I. Martínez Gamba and M.C. Jorge Squeff, Simulation of the transient behavior of a one-dimensional semiconductor device, Mat. Apl. Comput. 5 (1986) 103–122.
[27] J. Douglas, Jr., F. Pereira and L.-M. Yeh, A parallelizable method for two-phase flows in naturally-fractured reservoirs, Computational Geosciences 1 (1997) 333–368.
[28] J. Douglas, Jr. and T.F. Russell, Numerical methods for convection-dominated diffusion problems based on combining the method of characteristics with finite element or finite difference procedures, SIAM J. Numer. Anal. 19 (1982) 871–885.
[29] J. Douglas, Jr. and Y. Yuan, Numerical simulation of immiscible flow in porous media based on combining the method of characteristics with mixed finite element procedures, in: *Numerical Simulation in Oil Recovery*, The IMA Volumes in Mathematics and its Applications, Vol. 11, ed. M.F. Wheeler (Springer, Berlin, 1988) pp. 119–131.
[30] R.E. Ewing, T.F. Russell and M.F. Wheeler, Convergence analysis of an approximation of miscible displacement in porous media by mixed finite elements and a modified method of characteristics, Comput. Math. Appl. Mech. Engrg. 47 (1984) 73–92.
[31] F. Furtado and F. Pereira, Scaling analysis for two-phase, immiscible flow in heterogeneous media, Comput. Appl. Math. 17 (1998) 233–262.
[32] F. Furtado and F. Pereira, Mixing regimes and the scale up problem for multiphase flow, in: *Computational Methods in Water Resources XII*, Vol. 2 (1998) pp. 83–90.
[33] F. Furtado and F. Pereira, Fluid mixing regimes for two-phase flow in heterogeneous porous media, submitted.
[34] J. Glimm, B. Lindquist, F. Pereira and R. Peierls, The fractal hypothesis and anomalous diffusion, Mat. Apl. Comput. 11 (1992) 189–207.
[35] J. Glimm, B. Lindquist, F. Pereira and Q. Zhang, A theory of macrodispersion for the scale up problem, Transport in Porous Media 13 (1993) 97–122.
[36] C.S. Huang, The modified method of characteristics with adjusted advection and an accelerated domain decomposition procedure, Ph.D. thesis (July 1998); currently available as Technical Report #318, Center for Applied Mathematics, Purdue University, and to appear in Computational Geosciences.
[37] C. Johnson, Streamline diffusion methods for problems in fluid dynamics, in: *Finite Elements in Fluids* IV (Wiley, New York, 1993) pp. 97–122.
[38] J.C. Nedelec, Mixed finite elements in $\mathbf{R}^3$, Numer. Math. 35 (1980) 315–341.
[39] D.W. Peaceman, Improved treatment of dispersion in numerical calculation of multidimensional miscible displacement, Soc. Petroleum Engrg. J. 6 (1966) 213–216.
[40] P.-A. Raviart and J.M. Thomas, A mixed finite element method for second order elliptic problems, in: *Mathematical Aspects of the Finite Element Method*, Lecture Notes in Mathematics, Vol. 606, eds. I. Galligani and E. Magenes (Springer, Berlin, 1977) pp. 292–315.
[41] T.F. Russell, An incompletely iterated characteristic finite element method for a miscible displacement problem, Ph.D. thesis, University of Chicago, Chicago (1980).
[42] T.F. Russell, Time stepping along characteristics with incomplete iteration for a Galerkin approximation of miscible displacement in porous media, SIAM J. Numer. Anal. 22 (1985) 970–1013.
[43] A.M. Spagnuolo, Approximation of nuclear contaminant transport through porous media, Ph.D. thesis (July 1998); currently available as Technical Report #319, Center for Applied Mathematics, Purdue University, and to appear in Computational Geosciences.
[44] J.M. Thomas, Sur l'analyse numérique des methodes d'éléments finis hybrides et mixtes, Thèse, Université Pierre et Marie Curie, Paris (1977).